Pergamon

Geochimica et Cosmochimica Acta, Vol. 68, No. 11, pp. 2417–2435, 2004

0016-7037/04 $30.00 + .00

doi:10.1016/j.gca.2003.08.010

Heterogeneous reduction of uranyl by micas: Crystal chemical and solution controls

EUGENE S. ILTON,[1,*] ANCA HAIDUC,[2] CARL O. MOSES,[3] STEVE M. HEALD,[4] DAVID C. ELBERT,[5] and DAVID R. VEBLEN[5]

[1]Pacific Northwest National Laboratory, PO Box 999, MSIN: K8-96, 902 Battelle Blvd., Richland, WA 99352, USA
[2]Shell Global Solutions International B.V., P.O. Box 38000, 1030 BN Amsterdam, The Netherlands
[3]Lehigh University, Department of Earth &Environmental Sciences 31 Williams Drive Bethlehem, PA 18015, USA
[4]PNC-CAT, Bldg. 435E, 9700 S. Cass Ave., Argonne, IL 60439, USA
[5]Department of Earth and Planetary Sciences, The Johns Hopkins University, Baltimore, MD 21218, USA

(*Received April* 16, 2003; *accepted in revised form August* 19, 2003)

Abstract—This contribution primarily uses X-ray photoelectron spectroscopy (XPS) to better understand mechanisms for coupled sorption-reduction of aqueous U^{VI} by ferrous micas. Additional information was obtained with X-ray absorption spectroscopy (XAS) and transmission electron microscopy (TEM). The research is important because homogeneous reduction of aqueous U^{VI} is sluggish compared to heterogeneous reduction pathways, and micas are important sorbents for uranium in granitic terrains, which have been proposed as potential radionuclide waste disposal sites.

Three micas (high, medium and low Fe/Mg biotites), prepared as thin centimeter-sized books, were reacted with U^{VI} solutions that contained 0–25 mM Na^+ or K^+, at pH = 4.5, 5.0, 6.0, and 9.5. All the experiments were performed under argon at one bar. Solid samples were retrieved at timed intervals for up to 20 h. Both mica edge and basal plane orientations were analyzed by XPS. Analyses of peak positions, core satellites, and the 5f valence band indicate that U^{VI} can be reduced by biotite and that heterogeneous reduction depends on the type and concentration of alkali cation in solution, crystallography, and mica composition. We conclude that ferrous micas can reduce U^{VI} on edge sites, but not on exposed basal plane surfaces, and that Na^+ and K^+ facilitate and hinder the reaction, respectively. These observations pertain over a broad range of pH.

X-Ray absorption near edge spectroscopy (XANES) of annite sections indicates that the interlayer region, as opposed to external basal surfaces, also offers possible sites for heterogeneous reduction of U^{VI}. TEM of annites with high uranium coverage confirmed the presence of interlayer uranium; interestingly, this uranium is concentrated in U-rich nano-scale zones.

1. INTRODUCTION

Over the past 50 years there has been an intense effort to characterize the interaction of U^{VI} with geological materials. The motivation has stemmed from dual desires to find and exploit uranium ore deposits and to isolate long-lived radionuclide wastes. The primary goal of this contribution is to determine whether Fe^{II}-bearing micas can sorb and reduce aqueous U^{VI} to U^{IV}. Phyllosilicates are known sorbents for aqueous U^{VI}, and some of the rock-forming species are ubiquitous reservoirs of Fe^{II}, a possible reducing agent for U^{VI}. Reduction of soluble U^{VI} to less-soluble U^{IV} is a mechanism for limiting the mobility of U in the environment (e.g., Langmuir, 1978). The interaction of uranyl with micas is an important determinant of the mobility of U in granitic terrains, which have been proposed as radionuclide waste disposal sites. Heterogeneous reduction mechanisms for U^{VI} are particularly important, because homogeneous reduction of aqueous U^{VI} is sluggish (Wersin et al., 1994, and references therein; Liger et al., 1999).

The literature on clay minerals is relevant because of gross structural similarities with micas. There have been numerous experimental studies on the interaction of U^{VI}_{aq} with layer-silicate clays (Goldsztaub and Wey, 1955; Giblin, 1980; Borovec, 1981; Giblin et al., 1981; Tsunashima et al., 1981; Ames et al., 1982, 1983a; Andersson et al., 1982; Chisholm-Brause et al., 1992, 1994; Dent et al., 1992; McKinley and Sholtis, 1993, and references therein; Vandergraaf et al., 1993, see references therein; Hudson et al., 1994; Morris et al., 1994; Ticknor, 1994; McKinley et al., 1995; Ticknor et al., 1996; Giaquinta et al., 1997; Turner et al., 1996; Morris et al., 1997; Pabalan and Turner, 1997; Redden et al., 1997; Akcay, 1998; Pabalan et al., 1998; Thompson et al., 1998; Nero et al., 1999; Syed, 1999). None of these studies, however, addressed heterogeneous reduction of U^{VI} by structural Fe^{II}. In an EXAFS study of U^{VI} sorption by vermiculite and hydrobiotite, Hudson et al. (1999) state that U^{VI} is not reduced to U^{IV}. The Fe^{II} contents of the minerals were not given, however, and experimental conditions might not have been conducive to reduction (i.e., O_2 and CO_2 were present; CO_2 restricts the stability field of U^{IV}-containing compounds).

The literature for experimental studies on the interaction of aqueous U^{VI} with powdered rock-forming phyllosilicates is less extensive than for clays (Allard et al., 1979; Anderson et al., 1982; Ames et al., 1983b; Ticknor, 1994; Idemitsu et al., 1995; Mainka et al., 1999; Moyes et al., 2000). Although heterogeneous reduction of U^{VI} by ferrous silicates was considered to be potentially important in the above studies, no effort was made with advanced analytical techniques to determine whether or not such a reaction occurred, or to explore conditions under which heterogeneous reduction might be favorable. Idemitsu et al. (1995) noted that some U was sorbed irreversibly on biotite and postulated that this fraction represented U^{IV}. The lack of direct evidence for U^{IV}, however, compromises this conclusion of their study.

A number of studies have used micro-analytical techniques

* Author to whom correspondence should be addressed (Eugene.Ilton@PNL.gov).

(including Rutherford backscattering spectroscopy) to study the sorption of U^{VI} on micas and chlorite in polished-rock thin sections (Dran et al., 1988; Berry et al., 1989, 1991, 1993, 1994, 1995; Smyth et al., 1980). Two interesting findings for granitic rocks were that (1) biotite and chlorite concentrated U relative to the non-mafic assemblage and (2) the sorption of U depended on mica orientation and increased with increasing exposure of edges as opposed to basal-plane surfaces. The possible reduction of U^{VI} on the mica surfaces was not addressed.

Eberly et al. (1995) noted a close spatial relationship between uraninite and Fe-bearing chlorite in hydrothermal veins associated with the natural nuclear reactor at Bangombe, Republic of Gabon. Based on the textural relationship between uraninite and chlorite, Eberly et al. (1996) suggested that chlorite heterogeneously reduced aqueous uranyl to U^{IV} in uraninite.

Wersin et al. (1994) and Liger et al. (1999) demonstrated that pyrite and Fe^{II} adsorbed to α-Fe_2O_3 can heterogeneously reduce U^{VI} to U^{IV}. O'Loughlin et al. (2003) showed that a mixed Fe^{II}/Fe^{III} hydroxide (green rust) reduced U^{VI} to U^{IV}. In contrast, there is no definitive proof for U^{VI} reduction by structural Fe^{II} near mica or clay surfaces. In addition, previous workers have not considered the effects of alkali cations on the heterogeneous reduction of U^{VI} by sheet silicates. Reduction of metals at the biotite edge-fluid interface is strongly dependent on the concentration and type of alkali metal in solution (Ilton and Veblen, 1994; Ilton et al., 1997, 2000).

The objectives of this contribution are to determine (1) whether ferrous micas can sorb and reduce aqueous U^{VI} to U^{IV}, (2) whether the type of alkali cation in solution affects the redox reaction, and (3) whether reduction occurs on edge, exposed basal surfaces, or in the interlayer region. Large single crystals of mica were studied so that edge and basal plane orientations could be analyzed by X-ray photoelectron spectroscopy (XPS). XPS is a surface-sensitive spectroscopy that can distinguish between U^{IV} and U^{VI}; previous studies have demonstrated the ability of XPS to determine the oxidation state of U from natural environments (Sunder et al., 1992, 1994, 1996) and in experimental assemblages (Sunder et al., 1981, 1990; Wersin et al., 1994; Sunder and Miller, 1995; Guilbert et al., 2000, 2002). X-ray absorption spectroscopy (XAS) and transmission electron microscopy (TEM) provided additional information.

2. MATERIALS AND METHODS

2.1. Materials

U^{VI} solutions were prepared by adding $UO_2(NO_3)_2 \cdot 6H_2O$ (Reagent grade) to deionized water (electrical resistivity at 25°C > 16.6 mol/Ω cm^{-1}). The pH was adjusted with reagent grade NaOH or KOH. Reagent grade NaCl and KCl were added as needed.

Three different mica specimens were used in the experiments: a low and a medium Fe biotite came from Bancroft, Ontario (Wards Scientific), and a nearly pure Fe biotite (Annite) from Mt. St. Hilaire, Quebec was purchased from Excalibur Minerals. Compositions are given in Table 1. All mica blocks used in the experiments were sectioned from interior portions of large mica books. X-ray diffraction, optical microscopy, and spot checks with transmission electron microscopy did not detect weathering. Minor amounts of quartz and calcite inclusions were judged to be inconsequential. The mica books were sectioned into roughly $1.5 \times 0.5 \times 0.3$ cm blocks with a 0.004″ diamond-wafering blade (stainless steel) on an Isomet slow-speed saw. Deionized water with 25 mM KCl was used as the lubricant. KCl was added to minimize oxidation of Fe^{II} in the biotite during sectioning. The inhibitory effect of K on oxidation of structural Fe^{II} in micas is well documented (Scott and Amonette, 1988 and refs. therein). The sectioned books were sonicated in a fresh batch of KCl solution and then rinsed in a stream of de-aerated deionized water in an argon filled glove bag. Excess water was vigorously blown off with an Ultrajet Aerosol Duster (Chemtronics). The micas were then dried and stored under vacuum in a desiccator.

Table 1. Bulk chemical analyses of initial mica compositions.

	Si	Al	Mg	Fe	Ti	K	Na
L	3.04	0.95	1.98	0.74	0.14	0.91	0.08
M	3.00	0.96	1.56	1.14	0.11	0.92	0.07
A	2.90	0.97	0.05	2.80	0.07	0.94	0.05

L and M are from Bancroft, Ontario (Wards Scientific). A designates Annite from Mt. St. Hilaire, Quebec (Excalibur Minerals). Electron microprobe analyses given as atomic proportions assuming a total anion charge of 22.

The preparation procedure may have produced artifacts, such as point or line defects, that might not be present in naturally terminated mica crystals. These potential defects may have accelerated or hindered the absolute reaction rates and affected the distribution of U among the various possible sorption sites. In addition, despite the precautions taken, it is possible that some oxidation of surficial Fe^{II} occurred. However, as all the specimens were prepared in an identical fashion, we assume that differences in reaction rates and U4f binding energies (BEs) between experiments were not related to preparation artifacts.

To test whether preparation actually caused electron transfer to occur, a subset of annites were preleached for 24 h, before reaction with uranyl, at pH 4.5 in 25 mM NaCl solutions under an inert atmosphere (argon at 1 atm.). The intent was to simulate partially weathered micas that have expanded interlayer regions and to anneal potential high energy sites that may, or may not, facilitate electron transfer.

Basal plane surfaces were obtained by splitting the cut biotite wafers along 001 with a razor blade. Often, step edges were exposed or possibly created on the basal surface. These surfaces provided another means to test whether electron transfer is an artifact of preparation.

2.2. Experimental

The experiments were conducted in continuously stirred 50–500 mL polypropylene containers. Before the experiments, all plasticware was boiled in de-ionized water to remove any remnant volatile plasticizers, HCl/HNO_3-washed, and rinsed in de-ionized water.

Solution compositions covered pH 4.5–9.5, Na or K = 0 to

25 mM, and U^{VI} = 0.5 μM to 0.5 mM. All experimental procedures were performed under argon at 1 bar in a glove box. Measured temperatures varied from 24° to 26°C. Argon was 99.999% pure and used as supplied. Solutions were purged with argon before insertion of the mica. No effort was made to ensure that the experiments were strictly anaerobic. pH was measured before and after each experiment and aqueous metal concentrations were analyzed with an ARL 34000 inductively coupled plasma atomic emission spectrophotometer. The mica books were sequentially extracted from the experiments at designated reaction times, from 1 to 20 h, using vacuum-pipette tweezers, and immediately rinsed in a stream of de-ionized water. Excess water on rinsed mica books was suctioned off with the vacuum pipette. The mica books were then dried and stored under vacuum in a desiccator. The desiccator was then placed in an N_2 or Ar-filled glove bag attached to the entry port of the XPS instrument such that the samples were transferred into the XPS with minimal exposure to oxygen.

2.3. X-Ray Photoelectron Spectroscopy

XPS analyses were performed with a Scienta ESCA-300, which employs a high flux of monochromatic Al Kα X-rays. The analyzer operating parameters of 300 and 150 eV pass energy and a 1.1 mm slit yielded a Fermi level width of 0.66 and 0.41 eV for Ag, respectively. Pass energies of 150 eV were used for high concentrations of sorbed U. The relatively high pass energy of 300 eV optimized the balance between energy resolution and peak sensitivity for low amounts of sorbed U. A monochromatic low-energy electron flood gun was used to help neutralize charge build up at the sample surface. Spectra were acquired at a 90° takeoff angle and consisted of high-resolution regional scans over line positions of the elements of interest. Angle-resolved analyses of edge orientations were not possible, due to surface roughness. The analytical area was about 8 mm $\times$ 300 μm.

U peak positions were referenced to the binding energy (BE) of C1s at 284.6 eV. Mica compositions were measured with U4f, Mg2p, Fe3p, Na2s, Al2p, Si2s and K2p peaks. Analyses were semiquantified by using Al Kα photoionization cross sections as first-order sensitivity factors (Scofield, 1976). The same background fitting procedure was used for each element from sample to sample (either linear or Shirley background, Shirley, 1972). Compositional data are presented as the atomic ratio of the element of interest to silicon. Normalization of compositional data to Si reduced variance caused by differential adventitious carbon and sorbed U from sample to sample. Si in biotite is conservative relative to all other cations at most of the experimental conditions (Acker and Bricker, 1992; Ilton et al., 1997, 2000).

2.3.1. Charge broadening

Because micas are electrical insulators, charge broadening is an issue. Non-monochromatic instruments produce a high flux of secondary electrons that help to charge-neutralize insulator surfaces. The instrument in this study produces a monochromatic X-ray beam and requires the use of a low-energy electron flood gun to help charge-neutralize insulators. In fact, peaks were not resolved without the use of the floodgun. Importantly, the flood gun allowed for standardization of the Si2p full-width-at-half-maximum. This minimized differential charge broadening between samples of the same mica type.

2.3.2. UHV and beam effects

Wersin et al. (1994) documented possible slow reduction of uranyl, adsorbed to sulfides, under ultra-high vacuum conditions. We have shown that uranyl sorbed to micas is reduced under the X-ray beam during XPS analysis, but not noticeably under UHV conditions alone. Accordingly, we minimized and standardized exposure of the samples to the X-ray beam. Although it is possible that some fraction of reduced U is produced by beam or UHV effects, differences in U^{IV} /U^{VI} ratios between samples reflect mineralogical or solution controls on the redox reaction.

2.3.3. Spectral modeling

U^{IV}/U^{VI} ratios were quantified by curve fitting U4$f_{7/2}$ spectra. For very low coverage of uranium, we curve fit the U4$f_{5/2}$ peak. This was necessary due to excessive interference from the K2s line for annite and both the K2s and Mg auger lines for the lower Fe biotites. Two component peaks (Gaussian-Lorenztian mix) with identical full-with-half-maximums (FWHM) representing U^{VI} and U^{IV} were used to model the composite U4$f_{7/2}$ peak. Peak parameters were derived from near end-member U^{VI} (uranyl precipitated on mica under air) and U^{IV} (a reduced uraninite) compounds, and compared favorably with literature values (see section 4.2). Optimum fits, however, required an additional two degrees of freedom for both component peak separation and FWHM. The reasons for this are discussed in section 4.2. Model K2s spectra were derived from XPS analyses of unreacted annite samples and used in the fitting of U4$f_{7/2}$ spectra. An additional peak was used to model U4$f_{5/2}$ spectra. This peak is a shakeup feature associated with the U^{VI} 4$f_{7/2}$ photoionization process and lies under the U4$f_{5/2}$ spectrum, 10 eV above the U4$f_{7/2}$ core level. We used our near end-member U^{VI} standard (see above) to model its peak parameters. It is well known that U^{VI} and U^{IV} have shakeup satellites at 4 and 10 eV, and 6.7 eV, respectively, above their core 4f levels (Allen et al., 1987; Pireaux et al., 1977). Ideally we would have included all these satellites in spectral modeling. However, the satellite features were not resolved at low uranium coverage. Consequently, for consistency, we only modeled the core peaks except for the U^{VI} satellite that was known to lie directly underneath the 4$f_{5/2}$ level.

2.4. X-Ray Absorption Spectroscopy

The X-ray microprobe measurements were made at the PNC-CAT beamline 20-ID at the Advanced Photon Source, ANL, using Kirkpatrick-Baez mirrors for focusing (Heald et al., 2001). The beam was focused to 1.5 μm horizontally and 1.7 μm vertically. The sample was oriented with a 45° angle with respect to the beam. Thus, the effective horizontal beam size is 2.1 μm. The beam energy was set to 17200 eV to excite the U L_α fluorescence line. At this energy the beam penetrated the sample (100 μm) with relatively little absorption. Because of

Table 2. Summary of X-ray photoelectron analyses for 5uM U(VI) experiments.

	pH	Alk(mM)	U/Si	U^{IV}/U^{VI}	K/Si	Fe/Si	Al/Si	Na/Si
1 hour								
A	4.5	0	0.009	0.39	0.19	0.92	0.33	n.d
A	4.5	25 Na	0.014	0.65	0.09	0.89	0.37	0.34
A	5.0	0	0.018	0.51	0.18	0.86	0.32	n.d
3 hours								
A	4.5	0	0.015	0.45	0.16	0.75	0.30	n.d
A	4.5	25 Na	0.026	1.18	0.12	0.91	0.36	0.28
A	5.0	0	0.016	0.41	0.20	0.87	0.31	n.d
A	5.0	25 Na	0.36	2.62	0.08	0.79	0.32	1.13
A	6.0	0	0.53	0.34	0.18	0.92	0.30	0.07
A	6.0	25 Na	0.62	1.02	0.13	0.91	0.35	1.86
A	9.5	0	0.25	0.38	0.20	1.08	0.33	0.15
A	9.5	25 Na	0.27	1.08	0.11	0.99	0.37	1.24
5 hours								
A	4.5	0	0.02	0.57	0.17	0.81	0.30	n.d
A	4.5	25 Na	0.04	1.57	0.07	0.79	0.33	0.36
A	4.5	5 Na	0.04	0.53	0.14	0.72	0.28	0.32
A *basal*	4.5	5 Na	0.002	0.26	0.01	0.56	0.25	0.02
A	4.5	25 K	0.003	n.d	0.28	0.83	0.29	n.d
A *basal*	4.5	25 K	0.001	n.d	0.24	0.88	0.30	n.d
A	5.0	0	0.02	0.52	0.17	0.77	0.28	n.d
A	5.0	5 Na	0.15	1.61	0.13	0.92	0.37	0.85
A	5.0	25 Na	0.71	2.40	0.09	0.71	0.39	1.79
A	5.0	25 K	0.002	0.02	0.27	0.94	0.33	n.d
20 hours								
A	4.5	0	0.02	0.29	0.14	0.52	0.21	n.d
M	4.5	0	0.002	0.16	0.16	0.31 (0.42 Mg)	0.28	n.d
A	4.5	25 Na	0.04	2.58	0.12	0.56	n.a	7.84
M	4.5	25 Na	0.001	0.16	0.13	0.29	0.25	0.08
A	4.5	25 K	0.01	0.06	0.29	0.75	0.31	0.04
A *prel*	4.5	0	0.25	0.35	0.04	0.73	0.34	0.22
A	5.0	0	0.02	0.41	0.18	0.82	0.25	n.d
A *basal*	5.0	0	0.02	0.14	0.03	0.23	0.14	n.d
A *basal*	5.0	0	0.02	0.08	0.03	0.23	0.14	n.d
M	5.0	0	0.005	0.03	0.17	0.28 (0.43 Mg)	0.26	0.01
L	5.0	0	0.004	0.03	0.18	0.21 (0.58 Mg)	0.25	n.d
A	5.0	25 Na	0.83	2.52	n.d	n.d	n.d	—
M	5.0	25 Na	0.002	0.04	0.13	0.31 (0.42 Mg)	0.26	0.09
L	5.0	25 Na	0.001	0.01	0.17	0.22 (0.59 Mg)	0.27	0.08

A, M, and L indicate high Fe (Annite), medium, and low Fe biotite, respectively. n.d and n.a indicate not detected and not analyzed. All analyses are for edge orientations, unless *basal* is indicated. *Prel* indicates preleached annite.

the sample orientation, this penetration further degrades the horizontal resolution.

The fluorescence was detected using a 13-element Ge detector oriented 90° from the incident beam direction and a wavelength-dispersive crystal (wdx) detector [Microspec model WDX using a LiF 220 analyzer crystal] tuned to the U L_α line. The 13-element detector records the entire fluorescence spectrum, and windows were set to record the U, Ca, Ti, Mn, Fe, Rb, and Sr signals. The wdx detector has better energy resolution, and provided a very clean U signal uncontaminated by the nearby Rb K_α line.

3. RESULTS

3.1. Solutions

Analyses of starting and final solutions indicated no discernible change for total U, Na, Fe, Mg, or K. The pH stayed within 0.15 units of its initial value. These results were expected because of very low surface area/fluid ratios in the experiments.

3.2. X-Ray Photoelectron Spectroscopy

Tables 2 and 3 list all XPS analyses for edge and basal plane orientations of biotites reacted with uranyl bearing solutions. Unless noted otherwise, the ensuing discussion concerns edge orientations. We first discuss experiments with 5 μM U^{VI}. Timed experimental runs at pH 4.5 and 5 for annite show that uranyl sorption increases up to 5 h and then reaches a plateau with little, if any, further sorption (Fig. 1). Interestingly, at both pH values, sorption is enhanced in NaCl solutions relative to those with no added NaCl. In contrast, the addition of KCl strongly inhibits sorption relative to solutions with no added alkali.

The sorption characteristics of the annite as a function of pH are systematically different from pH 4.5 to 5 for solutions that contain NaCl compared to those that have no added alkali (Fig. 1). Experiments with no-added-alkali recorded only a marginal increase in sorption as pH increased from 4.5 to 5. In contrast, sorption appreciably increased over the same pH range in 25 mM NaCl solutions. Although data at pH values higher than 5

Table 3. XPS Analyses for 0.5 μM, and 0.5 and 0.05 mM U(VI) experiments.

	pH	Alk(mM)	U/Si	U^{IV}/U^{VI}	K/Si	Fe/Si	Al/Si	Na/Si
0.5 mM U(VI); 20 hrs								
M	4.5	0.8 Na	0.011	0.43	0.21	0.40 (0.49 Mg)	0.32	n.d
L	4.5	0.8 Na	0.014	0.26	0.24	0.22 (0.57 Mg)	0.28	n.d
L	4.5	0.8 K	0.010	0.05	0.21	0.22 (0.60 Mg)	0.29	n.d
L *basal*	4.5	0.8 Na	0.003	0.03	0.21	0.19 (0.50 Mg)	0.37	n.d
0.05 mM U(VI); 20 hrs								
M	4.5	25.0 Na	0.004	0.12*	0.10	0.28 (0.37 Mg)	0.26	0.11
L	4.5	25.0 Na	0.004	0.03*	0.16	0.20 (0.56 Mg)	0.26	0.18
A	4.5	0.0	0.026	0.34	0.18	0.73	0.29	n.d
0.5 μM U(VI); 20 hrs								
A	4.5	0.0	0.005	1.03	n.a	n.a	n.a	n.a
A	5.0	0.0	0.011	0.33	n.a	n.a	n.a	n.a

A, M, and L indicate high (annite), medium and low Fe biotite, respectively. n.a and n.d indicate not analyzed and not detected, respectively. Experiments at 0.5 mM U^{VI} were done in 50 ml solutions and no chloride, all other experiments performed in 500 ml solutions with either no added alkali or NaCl added. All edge analyses, unless *basal* indicated. * Near detection limit; results not significant.

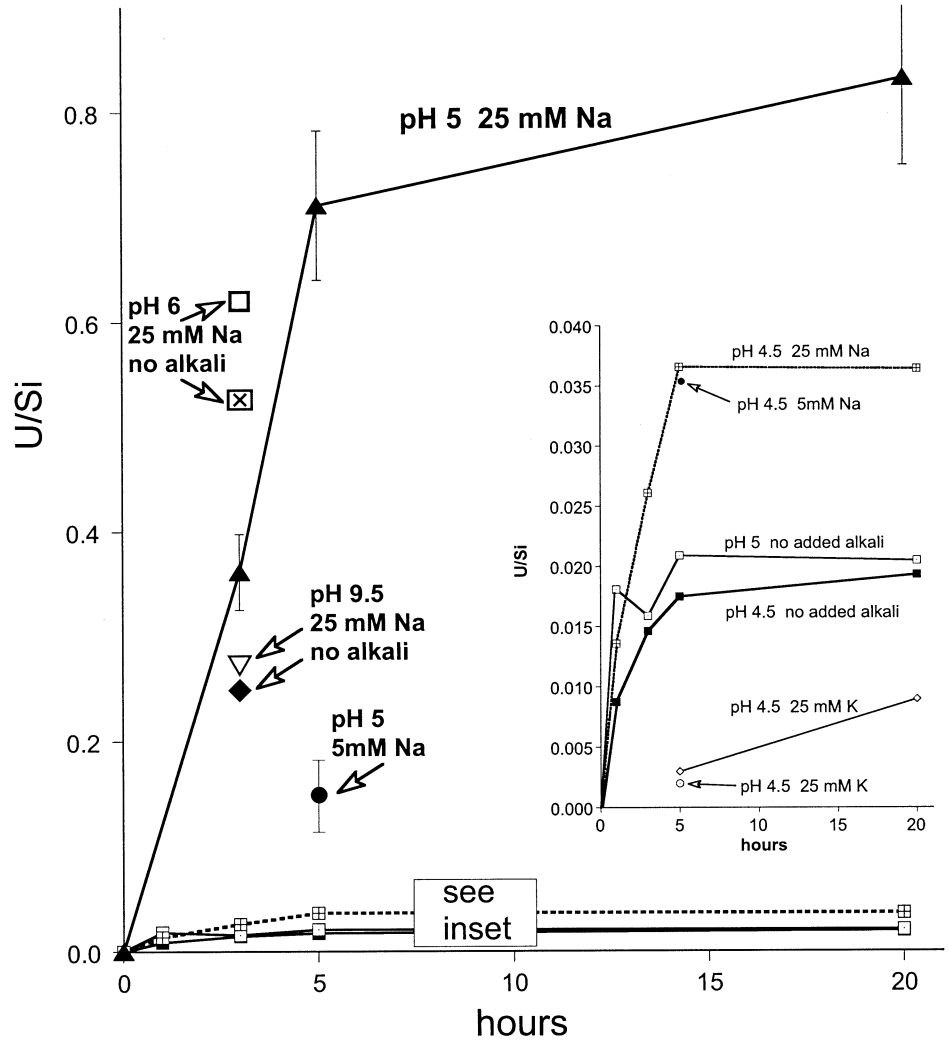

Fig. 1. XPS analyses of annite edge orientations showing uranium versus time after reaction with 5 μM U^{VI} solutions. The inset highlights the curves at lower uranium coverage.

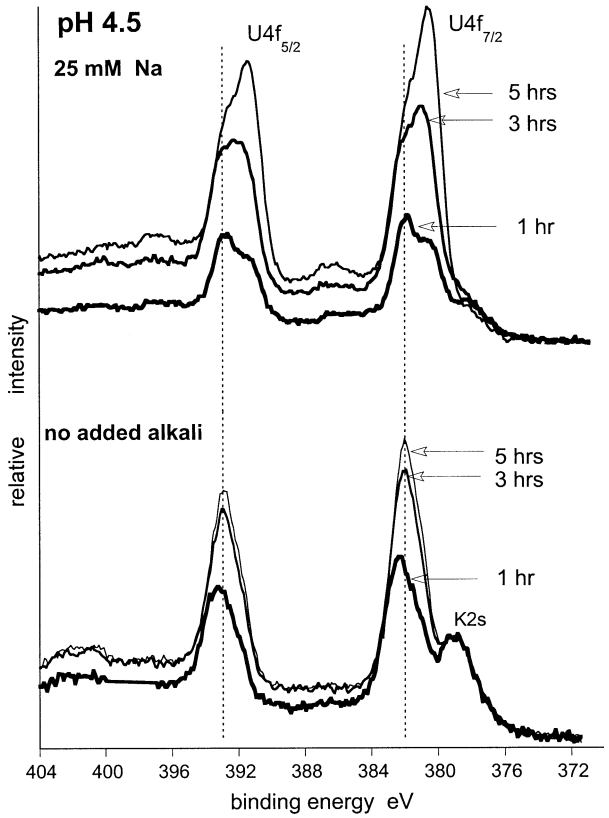

Fig. 2. XP spectra of the U4f region of annite edge orientations reacted with 5 μM U^{VI} that show evolution of the spectra with time. Note systematic spectral differences between the Na and no-added-Na experiments. The addition of Na appears to enhance growth of a low binding energy component. The vertical dashed lines correlate the high binding energy components in the U4f spectra between the 25 mM Na and no-added-alkali experiments. C1s set at 284.6 eV.

are limited to the 3 h reaction interval, both the Na and no Na experiments showed similar overall trends from pH 4.5 to 9.5: sorption appears to peak at about pH 6. Values at pH 7 and 8 are not shown due to pH instability and suspected homogeneous precipitation of uranyl.

Addition of alkali cations to solution strongly affected U4f peak shapes and positions for uranium sorbed by annite. These effects are similar at all pH values and time intervals. For example, at pH 4.5, $U4f_{7/2}$ and $U4f_{5/2}$ spectra for the Na experiments clearly show two components, where the low binding energy (BE) component grows with time (Fig. 2). In contrast, U4f spectra for the no Na experiments only show some asymmetry towards the low BE side (Figs. 2 and 3). Addition of K to solution further narrows and shifts the U4f spectra to even higher BEs relative to the no-added-alkali experiments (Fig. 3).

Total uranium sorption systematically increased from the low to the medium to the high Fe biotite (Fig. 4, Table 2). Further, U4f spectra for U sorbed on annite are consistently broader and shifted to lower BEs relative to the low and medium Fe biotites (Fig. 4, inset). Whereas differences between annite and the lower Fe biotites are obvious, U4f spectra for the low Fe biotite are only marginally narrower and slightly shifted to higher BEs compared to those for the medium Fe biotite.

Appreciably more U sorbed on edge compared to basal plane orientations (Fig. 5, top) and U4f spectra are consistently narrower and at higher BE for basal plane orientations than for edge orientations (Fig. 5, bottom). In contrast to edge orientations (Fig. 3), the shape and position of U4f spectra for basal plane orientations are not strongly affected by the presence or type of alkali cation in solution (Fig. 5, bottom).

The data set at 50 μM U^{VI} (Table 3) is much more limited than at 5 μM U^{VI}, but it is consistent with the results at 5 μM U^{VI}. The important point is that there is still no significant difference in U4f peak shapes between the low and medium Fe biotites.

It is only at 0.5 mM U^{VI}, another order of magnitude increase in uranyl concentration, that the lower Fe biotites display systematic and significant differences in U4f spectra as function of crystal chemistry, crystallography, and solution composition (Fig. 6). XP spectra of edge orientations reacted in Na solutions indicate that U4f spectra for the medium Fe biotite are broadened toward the low BE side compared to the low Fe biotite. For low Fe biotites, spectra are broader after reaction in Na- versus K-bearing solutions. The narrowest spectra are associated with U sorbed to the basal plane. In contrast, Mg2p, Fe3p, Al2p, and Si2p did not show asymmetrical broadening as a function of solution or mineral composition, or mica orientation. Consequently, at high uranyl concentrations, U4f spectral shapes for U sorbed by the low and medium biotites are the same function of solution and crystallographic parameters as they are for U sorbed by annite at lower uranyl concentrations.

3.3. X-Ray Absorption Spectroscopy

One annite thick section was analyzed by X-ray absorption spectroscopy (XAS) and the results are illustrated in Figure 7, which compares the fluorescent images obtained for U with total absorption. Note that the section is oriented with the 001 surface perpendicular to the page and with the reacted edge pointed north. The absorption is a measure of the sample thickness, and indicates the annite section is very uniform except for a few cracks. Note that the fluorescence signals are enhanced along the left hand edge. This is a result of the 45° sample orientation to the X-ray beam. Along this edge the escaping fluorescence photons penetrate less of the sample and suffer less absorption. For this reason the sample was oriented with the treated edge at the top. Away from the left hand edge the signal should be proportional to the U concentration. U is concentrated in a 10 μM thick fringe near the edge with weaker signals visible to a distance of 30–40 μm from the edge. Still, the highest U concentration is only about 10–20 ppm.

3.4. Transmission Electron Microscopy

High-resolution transmission electron microscopy (HRTEM) and analytical electron microscopy (AEM) of annite interior basal surfaces revealed nano-sized U-rich zones (Fig. 8). The U-rich zones only are observed in annites with high U coverage, as determined by XPS. Further characterization of these zones has been hampered by excessive sample drift at high magnification.

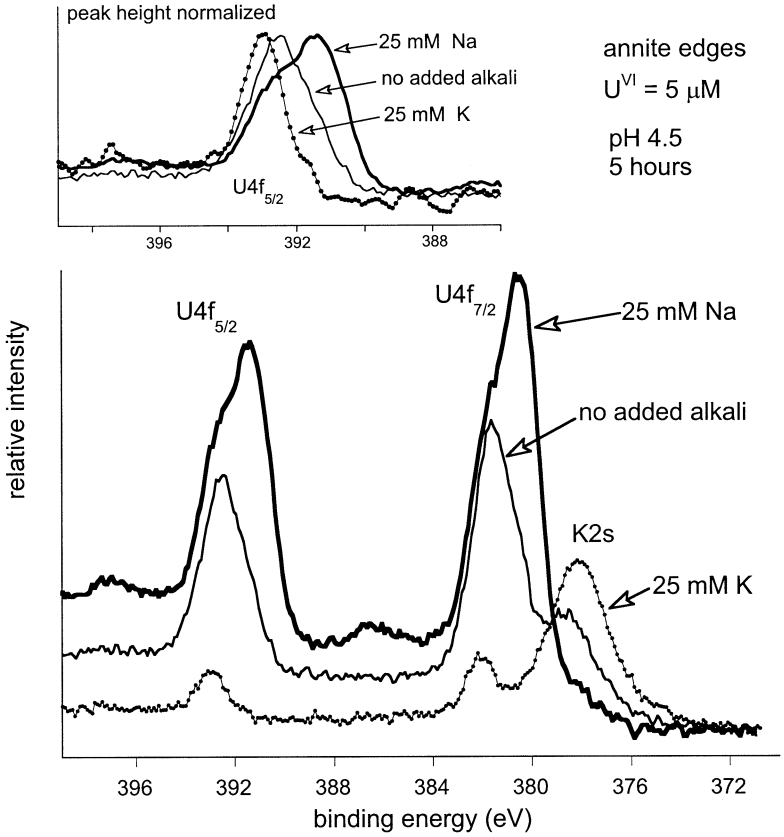

Fig. 3. XP spectra of the U4f region of annite edge orientations reacted with 5 μM U^{VI}. The inset highlights differences in peak shapes and position as a function of alkali cations in solution. Note that addition of K to solution both narrows and shifts U4f spectra to higher binding energies. This is opposite the effect of adding Na to solution. Binding energies were adjusted to C1s at 284.6 eV.

4. DISCUSSION

4.1. Bulk Thermodynamic Considerations

Figure 9 depicts Eh-pH relationships among mixed-valence U-oxides and some abundant U^{VI}_{aq} species for the CO_2-absent system as a function of uranyl concentration, calculated with thermodynamic data from Grenthe (1992). For systems equilibrated with atmospheric levels of CO_2, the formation of U^{VI} carbonate species with increasing pH, limits sorption and restricts the stability fields for mixed-valence U compounds. Because testing whether heterogeneous reduction occurs is the primary goal of this contribution, CO_2 was excluded from the experiments (as was O_2; see section 2.2). In any case, aqueous uranyl carbonate species only become dominant at pH greater than 6.4; consequently, we would not expect carbonate to significantly affect heterogeneous reduction of uranyl over the pH range 4.5 to 6, where the bulk of the experiments were performed. Whether uranyl-carbonato complexes sorb to mica surfaces, as occurs on hematite (Bargar et al., 2000), needs to be explored. The dashed horizontal lines mark the lower bracket for the redox potential of Fe^{II}/Fe^{III} in silicates given by White and Yee (1985). The shaded regions give the allowed pH range for reduction of U^{VI} to mixed-valence U oxides, given the unlikely assumption that the Eh for the structural Fe^{II}/Fe^{III} redox couple is independent of pH.

Predicting the conditions at which ferrous silicates heterogeneously reduce U^{VI} is complicated by a number of factors, including: (1) the lack of information concerning the Eh for the Fe^{II}/Fe^{III} redox couple in silicates as a function of solution and mineral compositions and (2) the application of bulk thermodynamic data for crystalline phases to possible reduced sorbed species or mixed-valent nano-scale precipitates that would be observed by XPS.

With these reservations in mind, reduction of U^{VI} by ferrous silicates is favored by increasing aqueous U^{VI} and pH $\approx$ 4–6. The accessible pH region is limited by the solubility of schoepite at higher U concentrations. A reasonable hypothesis is that, at low uranyl concentrations, only a narrow range of conditions is conducive to heterogeneous reduction of U^{VI} by ferrous micas; the reaction may not occur at $U^{VI} < 0.01$ m*M* concentrations or at low and high pH (Fig. 9). This hypothesis needs to be tested, as the implications for U mobility in the environment are important and the application of bulk thermodynamic data to heterogeneous redox reactions is uncertain.

4.2. XPS and XANES Evidence for U^{VI} Reduction

Curve fitting of annite XP spectra requires a minimum of two components. The question is whether those components represent different U^{VI} species or different oxidation states of uranium. At high U coverage, XP spectra of annite edge orienta-

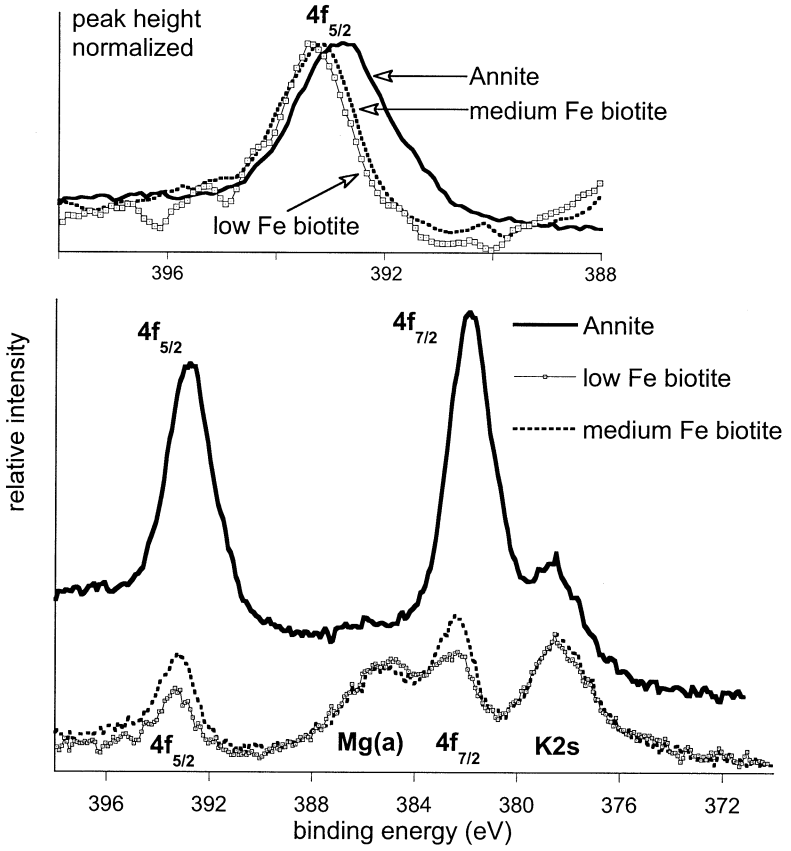

Fig. 4. XP spectra of the U4f region of mica edge orientations reacted with 5 μM U^{VI}. The inset highlights differences in peak shapes and positions as a function of biotite composition. Note that U4f spectra for the annite are clearly broader and shifted to lower binding energies than for the lower Fe biotites. In contrast, U4f spectra for the medium Fe biotite are only marginally broader and slightly shifted to lower binding energies than for the low Fe biotite. Binding energies were adjusted to C1s at 284.6 eV.

tions develop 5f peak intensity (Fig. 10a) and the appearance of satellite features at 6.0–6.7 and 4 eV above the low and high BE U4f component peaks, respectively (Fig. 10b). U^{VI} and U^{IV} have the electronic configuration $5f^0$ and $5f^2$, respectively, so the presence of 5f intensity signals that uranium is at least partially reduced. Further, many studies have shown that a 5.8–6.7 eV satellite is associated with UO_2 and is diagnostic of U^{IV}, whereas the satellites at 10 and 4 eV are diagnostic of U^{VI} (Table 4). The relationship between peak position and associated satellite features is illustrated in Figure 11 for near end-member U^{IV} and U^{VI} compounds. Because the intensities of the 5f peak and 6 eV satellite increase with increasing intensity of the low BE U4f component, we assign this component to U^{IV} (Figs. 10a,b). The high BE component is associated with satellites at 4 and 10 eV above the core peak (Fig. 10b). Because these satellites are associated with U^{VI} compounds (Table 4; Fig. 11), we assign the high BE component to U^{VI}. The U^{IV} and U^{VI} components are at 380.0–381.2 and 381.4–382.2 eV, respectively, giving separations that range from 1.0 to 1.5 eV. Absolute BEs for the component peaks are consistent, for the most part, with the range of BEs for U^{IV} and U^{VI} species (Table 4). Given appreciable uncertainty concerning the determination of absolute BEs for insulating materials, such as micas, a more important measure is the relative BEs of the component peaks. Interestingly, the BE difference between monovalent U^{IV} and U^{VI} compounds, for a given study, is 1.5–2.1 eV (Table 4), significantly higher than the BE separation between component peaks in our study. This suggests that mixed valence compounds formed on the biotite surfaces: Allen and Holmes's (1993) analysis of the mixed valent (U^{IV}–U^{VI}) compound U_3O_8 yielded a component peak separation of only 1.25 eV. Allen and Holmes invoked delocalization of electrons in mixed valent compounds to explain the smaller component peak separation relative to monovalent compounds. If true, component peak separations in mixed valent compounds could be a function of U^{IV}/U^{VI}. In fact, we found that optimum curve fitting required an extra degree of freedom for component peak separation. As noted above, optimum fits required BE separations in range 1.0–1.5 eV. As the TEM results are not definitive yet, and without additional information, the identity of the U^{IV}-containing species remains unknown.

In a few samples, however, the U^{IV} component appears at BEs around 381.2. This does appear too high, even with an error of 0.3 eV. Moreover, full-width-half-maximums (FWHM) for the component peaks, although the same for each component, varied from about 1.4 to 1.8 eV, with the majority clustered around 1.6 eV. No identified artifact accounts for this variability (e.g., FWHMs for biotite components are much less

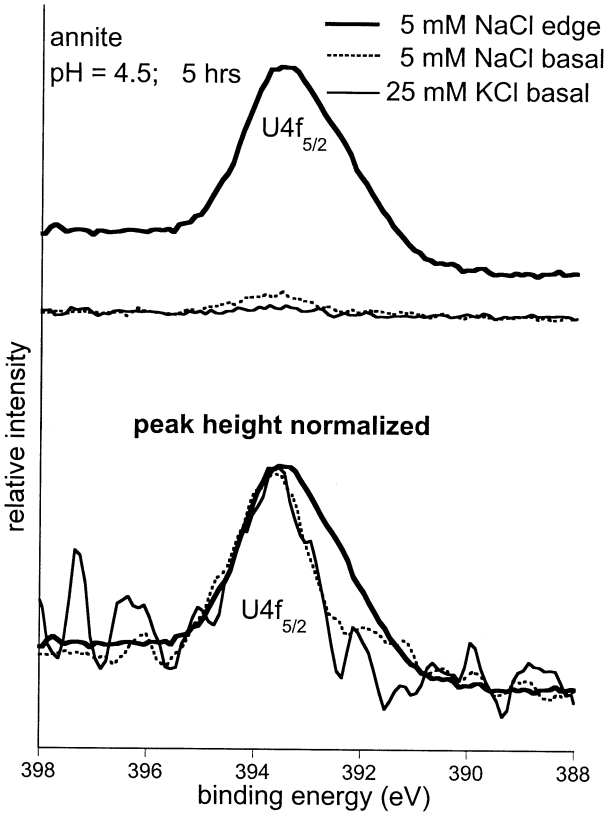

Fig. 5. XP spectra of the U4f region of annite edge and basal orientations reacted with 5 μM U^{VI}. Spectra at the top of the figure show appreciably more accumulation of U on edge compared to basal orientations. Peak height normalized spectra shows that U4f spectra for edge orientations are broadened to the low binding energy side relative to U4f spectra for basal orientations. Un-like edge orientations, addition of Na or K to solution has little effect on U4f peak shapes or positions for U sorbed to exposed smooth basal surfaces.

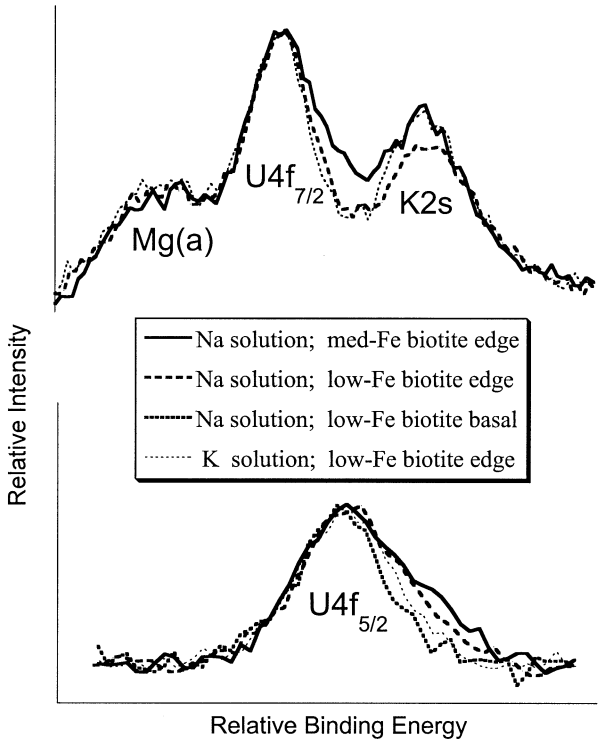

Fig. 6. XP spectra of edge and basal orientations of low and medium Fe biotites, after reaction with 0.5 mM U^{VI} for 20 h. The $U4f_{5/2}$ and $U4f_{7/2}$ regions from different samples were background subtracted using a Shirley type fit and peak-height normalized to either $U4f_{5/2}$ or $U4f_{7/2}$. The spectra show systematic broadening as a function of mineral and solution composition, and mica orientation.

variable). It is possible that a third species occurs in some spectra. Pentavalent uranium is a potential candidate. Proof of a U^{V} species would require, among other things, detailed analysis of satellite features, which is beyond the scope of this paper. As mentioned in section 2.3.3. satellite features are not accessible at lower uranium coverage.

XANES analyses of annite thick sections indicate that U^{VI} has been at least partially reduced to U^{IV}. Peak and edge positions as well as peak shapes are closer to a U^{IV} than a U^{VI} standard (Fig. 12).

For low U coverage, where noise to signal is too high to monitor the 5f level and satellite structures, U4f component peaks respond to changes in crystal chemical-solution parameters as at high uranium coverage. Consequently, we assume that monitoring the amount of the low and high BE component peaks yields information on the oxidation state of uranium across the entire range of uranium coverage.

Unambiguous evidence for reduction of uranyl on the low and medium biotites is manifest only at 0.5 mM U^{VI}. Quantitative curve fitting yields two primary component peaks separated by 1.3 eV, which is within the range of BE differences between U^{VI} and U^{IV} (Table 4), and is consistent with a mixed valence uranium compound as discussed above. U^{IV}/U^{VI} ratios, given in Table 3, show the same trend as a function of crystal structure and solution chemistry as the annites at lower U^{VI}_{aq}.

4.3. Crystal Chemical and Solution Controls on Sorption-Reduction

4.3.1. Background

Phyllosilicates are versatile sorbents, because they have two very different types of sorption sites: variably charged edge sites, similar to functional groups at oxide surfaces, and permanently charged sites on exposed basal planes and in the interlayer region that can act as exchange sites. Consequently, sorption of U^{VI}—an oxycation over a broad pH range—is governed by both edge and permanent charge sites. The degree of U^{VI} sorption by clay minerals, and presumably micas, is a function of pH-induced changes in mineral surface charge and aqueous speciation. Multiple binding-site modeling of uranyl sorption by montmorillonite (McKinley et al., 1995) has helped to constrain the effects of pH, uranyl hydrolysis, and ionic strength on the magnitude and site distribution of sorbed U^{VI}. Increasing ionic strength suppresses sorption by permanently charged exchange sites, and increasing pH favors sorption by variably charged edge sites relative to the fixed-charge sites. However, U^{VI} is still sorbed at edge sites at pH $\approx$ 4. Apparently, uranyl sorption is favored at aluminol relative to silanol edge sites. Interestingly, sorption at aluminol sites is best

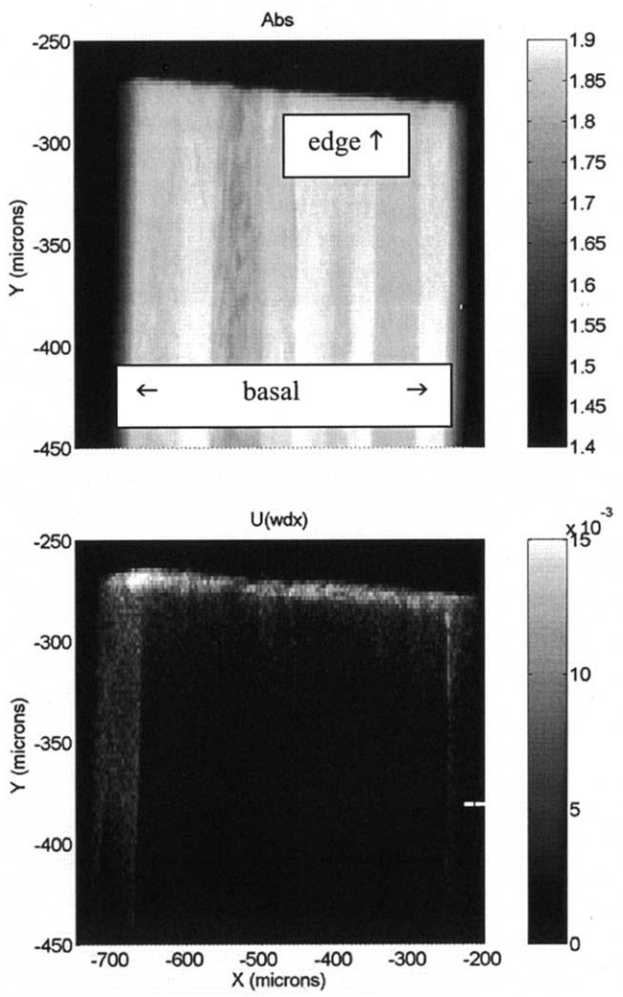

Fig. 7. X-ray absorption spectroscopy of annite thick section (100 μM thick). The annite was reacted for 5 h at pH 5 in a solution containing 5 μM U^{VI} and no added alkalis. Basal planes are oriented perpendicular to the page and the reacted edge is pointed north. Relative signal intensity is keyed to the grey-scale bar to the right of each figure. The top figure gives total absorption and is proportional to sample thickness. The bottom figure shows the fluorescence image for uranium. Uranium is concentrated in a 10 μM thick fringe at the reacted edge. The enhancement of uranium signal at the left edge of the sample is an artifact of sample orientation relative to the X-ray beam (see text).

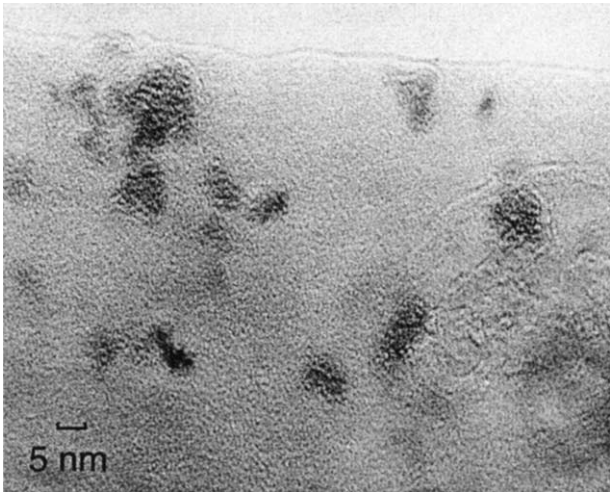

Fig. 8. TEM image of U-rich zones on interior basal surface of annite. The U zones are darker than the mica substrate. Note that the sample edge points north, but this edge might have been created during preparation and may not represent an edge that interacted with solution.

modeled with an $AlO \cdot UO_2^+$ species, even at high pH where the aqueous speciation is dominated by polynuclear species. At higher pH, saturation of aluminol sites allows oligomeric uranyl complexes at silanol sites. In situ spectroscopic studies of uranyl sorption by clay minerals (Chisholm-Brause et al., 1992, 1994; Dent et al., 1992; Morris et al., 1994; Thompson et al., 1998; Hudson et al., 1999; Sylwester et al., 2000; Hennig et al., 2002) have lent support to the modeling results, indicating that only the hydrated UO_2^{2+} species (similar to the aqueous species, but with some flattening in the equatorial plane) is present in the interlayer region, despite the presence of polynuclear species in solution, and that U^{VI} sorbs to edge sites via the inner-sphere complex $\cdot UO_2^+$. Polynuclear hydroxylated species adsorbed to edge sites are possible at higher pH. The spectroscopic results showing that U^{VI} sorbs to edges by an inner-sphere complex explain why U^{VI} sorbs to edge sites at $pH \ll pH_{pzc}$ (pH_{pzc} for montmorillonite edge sites is about 5.9—Charlet et al., 1993).

4.3.2. Reaction time

Timed experiments were performed on annite for solutions containing 5 μM U^{VI} at pH = 4.5 and 5. For the 25 mM NaCl solution at pH 4.5, U^{IV}/U^{VI} ratios increase with time; however, no significant trends are demonstrated at any other condition (Fig. 13). Because total sorption plateaus around 5 h, reduction essentially ceases after 5 h. In fact, for most experimental conditions, the bulk of reduction occurs in the first 3 h.

4.3.3. Mica composition

For any given solution composition, XPS analyses of edge orientations show that both absolute U concentrations and U^{IV}/U^{VI} ratios were appreciably higher on annite relative to the lower Fe micas (Table 2). At 0.5 mM uranyl, modeling indicates that significant U^{IV} occurs on both of the lower Fe micas, but that more reduction occurred on the medium relative to the low Fe mica (Table 3). The results are consistent with Fe concentration in biotite controlling uranyl reduction. This is not a surprise and was expected. However, the annite has much lower fluorine than the lower Fe micas. Fluorine is known to inhibit Fe^{II} oxidation in micas (Scott and Amonette, 1988, and references therein). Consequently, low fluorine likely contributed to the enhanced redox activity of the annite.

4.3.4. Crystallography

XPS of mica edge orientations and exposed basal surfaces show a strong anisotropy with respect to uranyl reduction and sorption; edge orientations have both higher total sorption and U^{IV}/U^{VI} ratios than basal orientations (Fig. 14). Further, the extent of reduction on exposed basal orientations was a func-

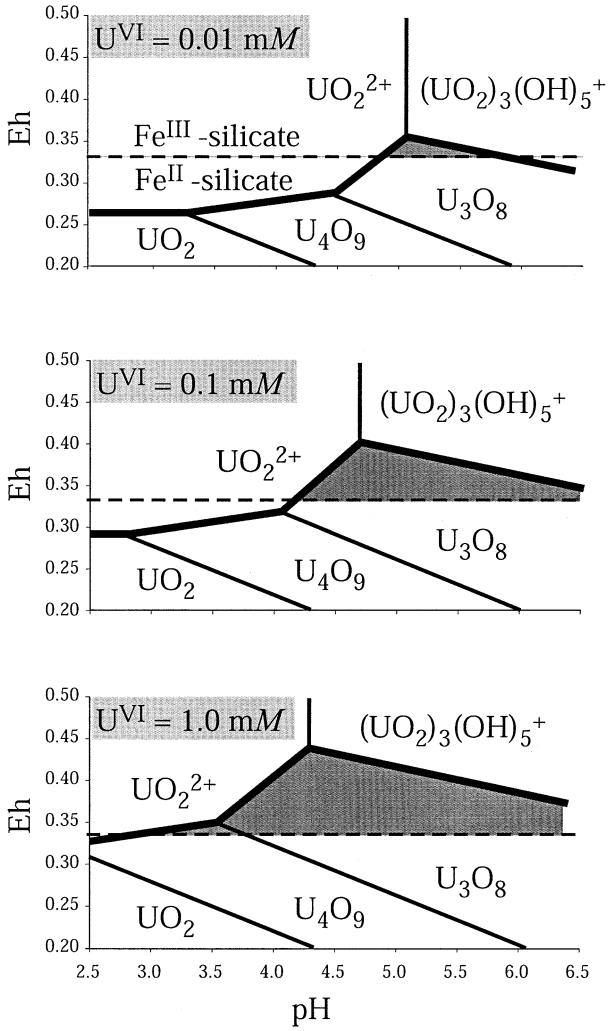

Fig. 9. Eh-pH stability diagrams for dominant U^{VI} aqueous species and mixed-valence U oxides at three different concentrations of aqueous U^{VI}. The horizontal line gives the lower bracket for the Fe^{II}/Fe^{III} redox couple in amphibole (see White and Yee, 1985, for applicable conditions). Thermodynamic data for U is from Grenthe (1992).

tion of surface roughness and likely associated with edge terminations at steps (Fig. 14). In contrast, XAS of annite sections (Figs. 8 and 13) yielded evidence for reduction of U^{VI} in the interlayer region.

4.3.5. Solution composition

Sorption-reduction of U by annite was very sensitive to the type and concentration of alkali cation in solution. At all pH values and reaction times, increasing aqueous Na^+ increased both total sorbed uranium (Table 2) and U^{IV}/U^{VI} (Figs. 15 and 16). An exception occurs for the 5 h experiment at pH 4.5 when going from 0 to 5 mM Na; however, due to error, this result is not significant. In contrast, K^+_{aq} severely restricts both sorption and reduction of uranyl on edge orientations relative to experiments with Na^+ and no-added-alkali. In fact, in the K experiments, sorbed U^{IV} is near the detection limit and sorbed U^{VI} is consistently lower, by orders of magnitude in some cases, compared to equivalent Na and no-added-alkali experiments. The difference in U^{VI} sorption between the Na and K experiments is, in part, a direct consequence of the well known high affinity of K, relative to Na, for the interlayer region of micas. This difference in affinity is due to the low hydration energy of K relative to Na which allows K to form strong inner sphere bonds with oxygens of opposing basal surfaces in the interlayer region, collapsing the interlayer region. In contrast, Na stays at least partially hydrated in the interlayer region and expands it (Sposito, 1984; Scott and Amonette, 1988). We infer that in the K experiments, K_{aq} maintained the collapsed state of the interlayer region making it less accessible to U^{VI}. This is consistent with K/Si ratios that approach unreacted bulk values (Table 2). In the case of mica, high Na^+ might facilitate uranyl sorption by exchanging with K^+ and causing interlayer hydration-expansion. Note that mica XPS analyses record appreciably lower K after reaction in Na solutions compared to the no-added-alkali and K experiments. In contrast, McKinley et al. (1995) showed that high Na depressed sorption of uranyl by montmorillonite at lower pH. The sorption characteristics of montmorillonite might differ from mica because its interlayer region is already in a hydrated/expanded state with Na occupying fixed charge sites.

A working hypothesis is that reduction should be more efficient (i.e., higher U^{IV}/U^{VI}) at low uranium coverage, or low U^{VI}_{aq}, due to a higher ratio of redox active sites relative to sorbed uranium. However, no systematic trends occurred.

XPS determined U sorption on edge orientations is generally consistent with batch sorption studies of phyllosilicates at high ionic strengths, where sorption sharply increases from pH 4 to 6 and then plateaus or decreases depending on the absence or presence of CO_2 (e.g., McKinley et al., 1995; Prikryl et al., 2001; Arnold et al., 1998). The decrease in total sorption from pH 6 to pH 9.5 (Fig. 16) possibly indicates that some CO_2 leaked into our system; aqueous uranyl carbonate species are relatively stable and tend to limit sorption (Langmuir, 1978). Alternatively, reduction could have altered the pH dependence of total U sorption. Although total sorption and total reduction were strong functions of pH (Fig. 16), it appears that reduction efficiency, as measured by the U^{IV}/U^{VI} ratio, was not (Fig. 15).

4.3.6. Summation of solution and crystal chemistry effects

The degree of heterogeneous reduction is influenced by crystallography, mineral composition, and the type of alkali cation in solution. Reduction of sorbed U^{VI} occurs on edge orientations, is at least partially blocked by the exposed siloxane sheet and by K in solution, is facilitated by aqueous Na and, as expected, increases with increasing Fe concentration in biotite. Total sorption increases from pH 4.5 to 5 for all reaction times. For the 3 h data set, total sorption increases from pH 4.5 to 6, then decreases at pH 9.5. U^{IV}/U^{VI} ratios show no systematic trend as a function of pH, within error, so total U^{IV} increases as total sorbed uranium increases.

Unlike the annite, the concentrations of sorbed uranium on the lower Fe micas is too low to detect the 5f level or satellite features diagnostic of reduced uranium. Still, the increase in the U4f low BE component is the same function of solution parameters and crystal structure and chemistry as for the annite. Based on the data and spectral modeling, and by

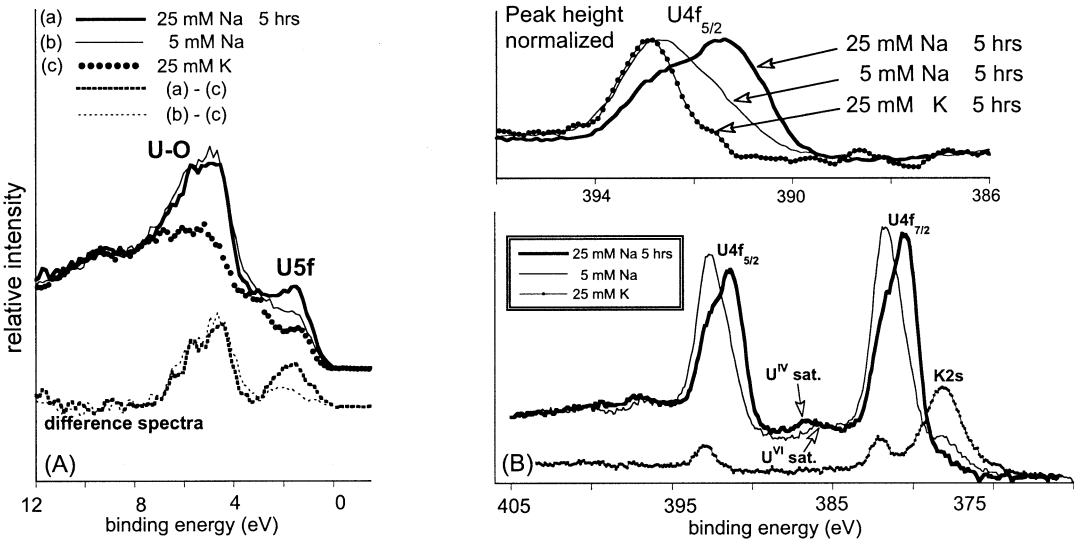

Fig. 10. XP spectra of the U4f region of annite edge orientations reacted with 5 μM U^{VI}. The purpose of this figure is to correlate certain features, such as satellites and U5f signal intensity, which are diagnostic of uranium oxidation state, with changes in core level U4f peak shapes and positions. These particular 5 and 25 mM Na experiments were chosen because nearly equivalent amounts of uranium were sorbed on both samples. Information from Figs. 10a,b demonstrates that increased U5f intensity is associated with the low binding energy component. Fig. 10b shows a strong association between the U^{IV} satellite and the low binding energy component, whereas a U^{VI} satellite is associated with the high binding energy component. As discussed in the text, these observations confirm that the low and high binding energy components are U^{IV} and U^{VI}, respectively. Binding energies were adjusted to C1s at 284.6 eV.

comparison with the behavior of the annite, we suggest that the low and medium Fe biotites can reduce U^{VI}. However, reduction of U^{VI} is detectable only at relatively high aqueous uranyl concentration (i.e., 0.5 mM), whereas annite can reduce uranium down to 0.5 μM, the lowest concentration used in this study.

Table 4. Binding energies for U(VI) and U(IV) compounds.

	$4f_{7/2}$	$4f_{5/2}$	Satellite	Notes
UO_2	380.2	391.1	6.8	Hedhili et al. (2000). Clean UO_2, no carbon
UO_2	379.8	390.7	—	Fiedor et al. (1998). C1s at 284.5 eV
$UO_2(NO_3)_2$ $6H_2O$	381.4	392.3	—	U^{VI}-U^{IV} = 1.6 eV
UO_2	380.8 (.1)	—	—	Wersin et al. (1994). Gold dot method. All samples
UO_3(amorph.)	382.4 (.2)	—	—	conducting. U^{VI}-U^{IV} = 1.6–1.4 eV
Uranyl on Fe_2O_3	382.2 (.25)	—	—	
UO_2	379.5 (.05)	390.4 (.05)	6.8 (.1)	Guilbert et al. (2000). C1s at 284.6 eV.
UO_3	381.6	—	—	With oxidation of UO2, satellite position diminishes to 5.8. U^{VI}-U^{IV} = 2.1 eV for endmembers and 1.1 eV for IV and VI components in UO_{2+x}
UO_2(thin layer)	380.1	390.9	—	Van den Berghe et al. (2001). C1s at 284.6eV.
UO_2(bulk)	380.0	390.8	6.8; 6.7	
$U0_{2.001}$	380.0 (.3)	—	—	Allen et al. (1974). Au at 84 eV.
γ - UO_3	381.9 (.3)	—	—	U^{VI}-U^{IV} = 1.9 eV
UO_3	—	—	3.7 & 10.6	Pireaux et al. (1977).
U_3O_8	—	—	—	Allen and Holmes (1993). C1s at 285.0(.1).
U^{IV} component	380.2	391.1	—	Conducting sample. C1s at 285.0(.1).
U^{VI} component	381.4	392.3	—	U^{VI}-U^{IV} = 1.2 eV.
UO_2	380.0 (.2)	390.9 (.2)	6.7	Ilton et al. (this study). C1s at 285.0(.2).
uranyl on mica	381.9 (.2)	392.7 (.2)	4 & 10	UO_2 is uraninite with some oxidation. Uranyl precipitated onto mica under air. U^{VI}-U^{IV} = 1.9 eV

Satellite positions given as eV above the core peak. Numbers in parentheses are errors provided by authors.

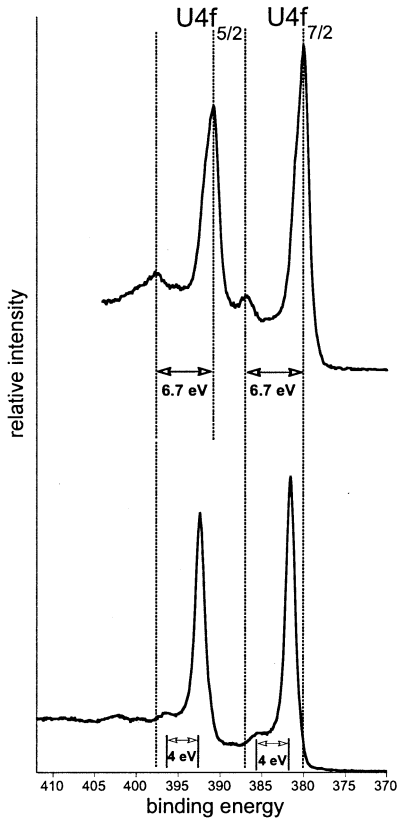

Fig. 11. XP spectra of the U4f region for a reduced uraninite (top spectrum) and uranyl precipitated on mica under air (bottom spectrum). Note the differences in core level and satellite positions between the uraninite and uranyl precipitate. BEs were adjusted to C1s at 284.6 eV.

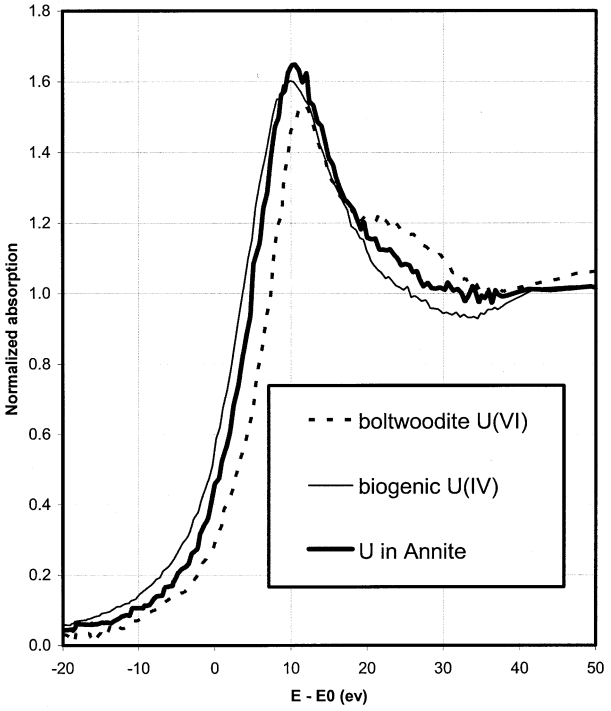

Fig. 12. XANES analyses of the same annite thick section (100 μM thick) shown in Fig. 7. The annite was reacted for 5 h at pH 5 in a solution containing 5 μM U^{VI} and no added alkalis. The spectrum for uranium in annite is closer to the U^{IV} standard (nano-sized crystals of UO_2 formed biogenically) than the U^{VI} standard (boltwoodite, a uranyl silicate).

4.4. Descriptive Models for Coupled Sorption/Reduction of U^{VI}

It should be kept in mind that the information depth for silicates using this XPS is about 80 Å with a lateral resolution of 300 μm by 5mm, XAS is providing bulk information with a lateral resolution of 2–5 μm, and TEM is yielding spatial (point to point) and analytical resolution on the order of 1.5 Angstroms and tens of cubic Angstroms, respectively. Consequently, each technique might highlight different aspects of the overall reaction and initially we discuss mechanistic models in the context of a particular technique. This is followed by a summary that attempts to stitch the observations from different scales into a coherent model. It will be shown that two different reduction mechanisms may be operative.

4.4.1. An XPS based model of U^{VI} sorption-reduction

XPS analyses showed that U^{VI} was detected on both edge and basal plane orientations, but that U^{IV} was detected only on edge orientations and rough basal surfaces. For an edge-site model of U(VI) sorption-reduction, it is reasonable to assume that U^{VI} sorbs to biotite edge sites under the experimental conditions; given that the calculated pH_{pzc} values and structure of biotite edges are similar to those for montmorillonite (Ilton et al., 1997). By analogy with spectroscopic and bulk sorption studies described in section 4.3.1, it is possible that uranyl sorbs to mica edge-sites (possibly aluminol sites or exposed Fe octahedra) as the inner-sphere complex $>O \cdot UO_2^{+}$. A two electron transfer reaction occurs, such that one sorbed U^{VI} is reduced to U^{IV} and two Fe^{II} in biotite are oxidized to Fe^{III}. In one scenario, two electrons could directly hop to uranyl, either simultaneously or in sequence, from two exposed Fe(II) octahedral that coordinate sorbed uranyl. Idemitsu et al. (1995)

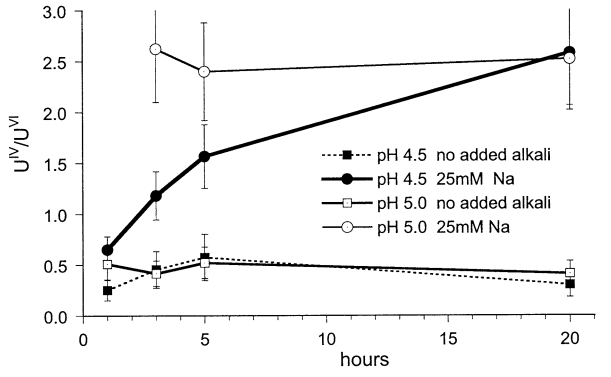

Fig. 13. Graph shows evolution of U^{IV}/U^{VI} ratios on edge orientations of annites as a function of reaction time for a given solution composition. All solutions contained 5 μM U^{VI}. Uranium oxidation states derived from modeling U4f XP spectra.

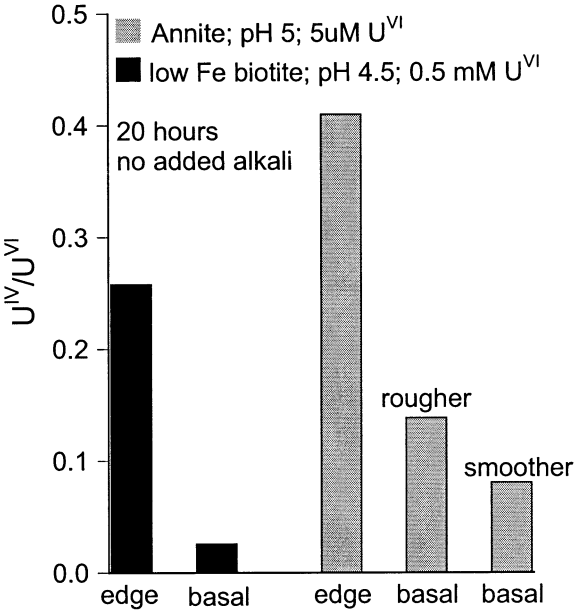

Fig. 14. Bar graph illustrates greater reduction of uranyl sorbed to edge orientations compared to external basal surfaces. Reduction on basal planes increases with increasing surface roughness. Uranium oxidation states were derived from modeling U4f XP spectra.

suggested a similar mechanism but postulated that defects on the basal plane that exposed edge terminations were the preferred reactive sites. In another scenario, the electrons could come from some variation of exposed and buried Fe(II) octahedra, which would necessitate solid state electron conduction along the octahedral sheet. Some hypothetical reactions are

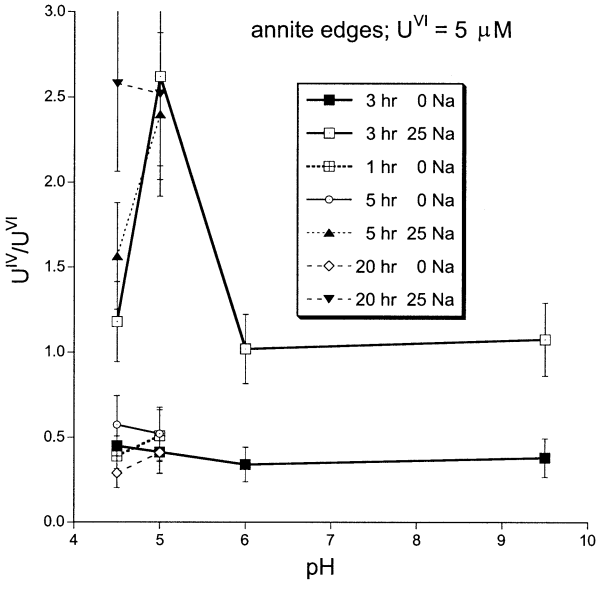

Fig. 15. Graph shows U^{IV}/U^{VI} ratios on edge orientations of annites as a function of pH for a given reaction time and solution composition. All solutions contained 5 μM U^{VI}. Uranium oxidation states were derived from modeling U4f XP spectra.

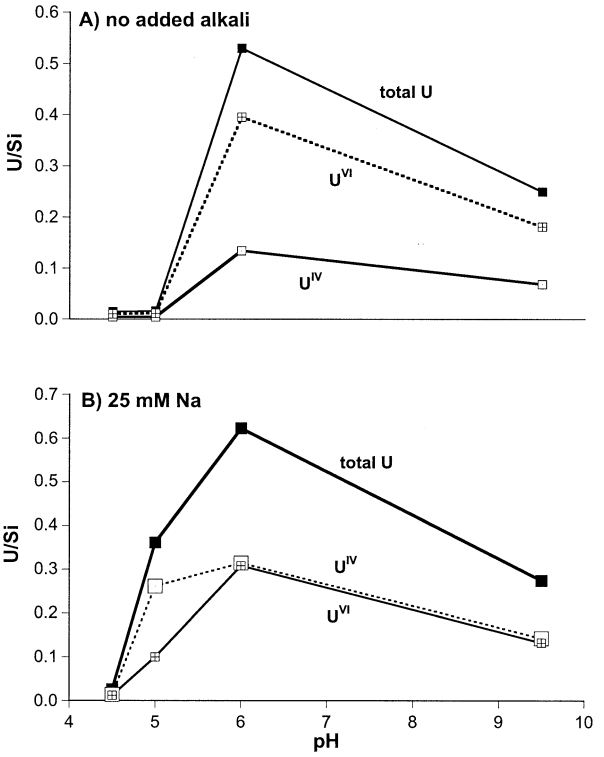

Fig. 16. Graph shows U/Si and $U^{IV\ or\ VI}$/Si ratios on edge orientations of annites as a function of pH for the 3 h reaction interval. All solutions contained 5 μM U^{VI}. Uranium oxidation states were derived from modeling U4f XP spectra.

1a.) $UO_2^{2+} + >OH_2^+ = >O \cdot U^{VI}O_2^+ + 2H^+$

1b.) $UO_2^{2+} + >OH = >O \cdot U^{VI}O_2^+ + H^+$

2.) $>O \cdot U^{VI}O_2^+ + 2H^+ + 2Fe^{II}_{bio} + 2M^+_{bio} = >O \cdot U^{IV}O^+ + H_2O + 2Fe^{III}_{bio} + 2M^+_{aq}$

3a.) $UO_2^{2+} + >OH_2^+ + 2Fe^{II}_{bio} + 2M^+_{bio} = >O \cdot U^{IV}O^+ + 2Fe^{III}_{bio} + H_2O + 2M^+_{aq}$

3b.) $UO_2^{2+} + >OH + H^+ + 2Fe^{II}_{bio} + 2M^+_{bio} = >O \cdot U^{IV}O^+ + 2Fe^{III}_{bio} + H_2O + 2M^+_{aq}$

Reactions 1a and 1b are the adsorption reactions, which assume that U^{VI} forms an inner-sphere complex at an edge site functional group, in accord with spectroscopic and sorption data of U^{VI} interactions with montmorillonite (see section 4.3.1). Reaction 2 is the heterogeneous redox reaction; U^{IV} is shown as an inner-sphere complex, although we know of no supporting data. One could complicate matters further by introducing mixed-valence reaction products. M is a cation that is released from biotite to maintain charge balance during oxidation of structural Fe^{II} (e.g., White and Yee, 1985; White, 1990). M could be any cation, including interlayer K^+ or H^+ from a hydroxyl group (Scott and Amonette, 1988; Fanning and Karamidas, 1977). Charge balance could also be maintained by sorption of negatively charged species such as OH^-. Combining reactions 1a and 2, and 1b and 2 yields coupled sorption-reduction reactions 3a and 3b, respectively.

The pH dependence of the overall reaction is a complicated function of U speciation and the protonated state of surface

functional groups (e.g., compare reactions 3a and 3b), whereas the charge-compensating cation, M, is an intrinsic feature. The fact that reduction of U^{VI} was hindered in K- relative to Na-bearing solutions suggests that K is the charge-compensating cation. However, K does not necessarily act directly as a charge-compensating cation; it is well known that, due to differences in hydration energy between Na and K, K^{+}_{aq} acts to prevent expansion/hydration of the mica interlayer region whereas at high Na/K ratios, Na^{+}_{aq} tends to hydrate and expand the interlayer region (see discussion in section 4.3.5). Interestingly, increasing hydration/expansion of the interlayer region as a function of Na/K is strongly correlated to oxidation of structural Fe^{II} by molecular oxidants (Scott and Amonette, 1988 and references therein). The effect of K and Na on heterogeneous mica redox reactions was also shown to apply to the heterogeneous reduction of chromate sorbed to biotite (Ilton et al., 1997). Interlayer expansion/hydration may hold the key to facilitating electron transfer reactions between micas and sorbed metals, either by providing fast diffusion pathways for electrons and charge compensating cations, or by allowing access of redox active species into the interlayer region (Ilton et al., 1997; Scott and Amonette, 1988; Amonette and Scott, 1995).

The simplistic comparison with uranyl adsorption experiments, described in section 4.3.5 may be fortuitous. For some experiments U/Si ratios approach 1 (Table 2) and annite signal has been significantly depressed. Suppression of annite signal suggests that the annite is under an overlayer. In contrast, the K^{+} experiments might yield true edge site sorption information because little to no reduction occurs in K solutions and K^{+} appears to block uranyl sorption by fixed charge sites (see discussion in section 4.3.5). Comparison of equivalent K and Na experiments shows that, in some cases, U/Si is over two orders of magnitude greater for annites reacted in NaCl relative to KCl solutions. To get a sense of how much uranium is at edge orientations at high coverages we used a simple model to estimate the sorption density in terms of equivalent monolayers of a one unit cell thick uraninite layer. Uraninite is appropriate because significant reduction occurred for the times series of experiments with annite at pH = 5, Na = 25 mM, and 5 μM uranyl. However, this monolayer is a purely hypothetical construct. Appendix A describes the model and assumptions. The calculations indicate that U/Si values of 0.02 to 0.3 correspond to about 1/4 to 2 monolayers of uraninite. Although these calculations are semiquantitative at best, they suggest that layer termination sites could be saturated at pH 6 and 9, and at pH 5 for 25 mM NaCl solutions. It is possible that U in the near surface interlayer region contributes signal to XPS analyses of edge orientations. This would lower the apparent saturation of edge sites. However, the pH behavior of total sorption is not what one would expect if fixed charge sites dominated the XPS resolved sorption characteristics of edge orientations. In fact, the "XPS sorption edge" (Fig. 16) mimics the sorption of uranyl by edge sites in the batch study of Mckinley et al. (1995). Still, this apparent correspondence does not necessarily imply a simple adsorption mechanism if the edge sites are saturated. A possible explanation for having more sorbed uranium than available sorption sites at edges (given that for most conditions the experiments were well below Schoepite saturation) is that reduction amplified uranyl adsorption by producing polymerized mixed valence oxide islands of uranium which created more sorption sites for uranyl. That mixed valence uranium compounds are good semiconductors implies that electrons could reach uranyl adsorbed to the polymerized surfaces. In this model, total sorption is limited by the reductive capacity of the mica, not mica adsorption sites. If so, the "XPS sorption edge" may simply preserve the initial conditions that favored uranyl adsorption to the layer terminations. The model predicts that a pure uranium (oxide-oxyhydroxide) phase or sorbate should accumulate on edges, which is consistent with results that record diminishing biotite signal with increasing uranium.

4.4.2. An XAS/TEM based model of U^{VI} sorption-reduction

XAS analyses of annite thick-sections show that sorbed uranium constitutes a 10 micron thick fringe at the biotite edge (Fig. 7), where maximum U concentrations only reach 10–20 ppm. XANES indicates that uranium is mainly in the U^{IV} oxidation state (Fig. 12). The easiest access into the interior is by transport along the interlayer region. If reduced uranium is in the interlayer region, then it is possible that electrons crossed the tetrahedral layer, as opposed to the edge termination model where electrons are transferred along the octahedral layer. Electron transfer across the tetrahedral layer to oxidants in the deep interlayer is the implied process for bulk oxidation of ferrous micas (Scott and Amonette, 1988, and references therein).

In contrast, XPS of external basal plane orientations indicated that reduction was correlated to roughness, or the density of step edges. This suggests that uranyl sorbed on exposed basal surfaces at frayed edges cannot be reduced by electron transfer across the tetrahedral layer, but does not necessarily rule out the possibility that uranyl is reduced in the interlayer region by this mechanism. If uranyl is reduced in the interlayer region, one needs to explain why it is not reduced on exposed basal surfaces. Although beyond the scope of this paper, steric effects (e.g., location of 2 nearest irons required for reduction to U^{IV}) and differences in layer charge experienced by uranyl in the interlayer versus exposed basal surfaces would be promising avenues to explore. Indeed, it appears that higher layer charge intensity can induce dehydration of uranyl sorbed to basal surfaces (Moyes et al., 2000), which may facilitate reduction.

An alternative explanation is that uranyl reduction actually occurs on edge terminations and the fringe of reduced uranium records the amplitude and abundance of off-set layers. At this point we cannot rule out either model; it is, of course, possible that a mixture of processes is producing the observed patterns of uranyl sorption-reduction. Higher spatial resolution techniques are necessary to elucidate the origin of the reduced uranium fringe, and distinguish between layer termination and interlayer region models for uranyl sorption-reduction. HRTEM of annite interior basal surfaces imaged nano-sized U-rich zones with no obvious crystal form and no apparent relationship to step edges (Fig. 8). Excessive vibration of the mica substrate, at high magnification, has precluded their identification. Despite no information on the oxidation state of uranium in these zones, the mere presence of uranium in the interlayer region, unassociated with steps, bolsters the possibility that XANES records

reduction of uranyl on interior basal surfaces as opposed to reduction of uranyl on offset edge terminations.

4.4.3. Summary

Two independent reduction reactions may be operative. An edge termination mechanism is supported by XPS observations, where reduced uranium accumulates on edge orientations. The process is distinguished by an inverse correlation between uranium and biotite components, including Fe. This suggests that a relatively pure uranium phase, possibly of mixed valence character (see section 4.2), is forming at edge terminations.

The evidence is consistent with no reduction of uranyl at smooth, external basal surfaces. In contrast, XAS and HRTEM observations are consistent with reduction of uranyl in the interlayer region, not at offset layer terminations. A more definitive model awaits the determination of both the identity and oxidation state of the nano-scale U-rich zones in the interlayer region.

4.5. Potential XPS Artifacts

4.5.1. Peak shapes and binding energies (BEs)

Where uranium sorption densities are high, features such as core shakeup peaks and 5f level intensity can directly identify U oxidation states. For low uranium coverage, however, oxidation states are determined by the BEs of modeled component peaks fit to the composite 4f spectra. Because XPS-determined BEs yield indirect information on the bonding environment of sorbed species, it is important to eliminate alternative explanations for BE shifts and peak broadening for the case of low U coverage. Tightly controlling experimental parameters and treating samples in identical fashion after extraction from solution helped to constrain the XPS data. For example, the three different micas were reacted in the same experimental solutions, which minimized the possibility that differential BE shifts in U4f among the micas were caused by different U^{VI} species. It is also unlikely that structural modifications of U^{VI} sorbed to different sites (e.g., edge versus interlayer sites), can account for spectral differences: XPS studies of UO_3 polymorphs indicate that the shapes and BEs of $U4f_{7/2}$ spectra are independent of coordination (Allen and Holmes, 1987). Slow reduction of U^{VI} under the beam and charge broadening were both minimized and normalized, so that differences in U4f spectral shapes cannot be due to UHV-induced reduction or differential charge broadening (see section 2.3.1). Consequently, the most likely explanation for peak broadening remains reduction of U^{VI} to U^{IV} at the mica-solution interface, not asymmetric charging. We cannot exclude, however, the possibility that a small percentage of U^{IV} is an artifact of beam-induced reduction.

4.5.2. Mica preparation

At issue is whether mica preparation (see section 2.1) influenced the redox activity of edge orientations. More specifically, will uranyl reduction occur on natural edge terminations or is reduction an artifact of defects created during the sawing procedure? To answer these questions we reacted both preleached mica edges and rough basal surfaces with aqueous uranyl. Micas were preleached to anneal high energy defects, potential sites of high redox activity, on edge orientations. Rough basal surfaces contained a high density of edge terminations that were occasionally exposed, or created, by splitting the books along 001. These steps on the basal surface should be more representative of "natural" edge terminations than their sawed counterparts. At the very least, they offer a chance to see if reduction is dependent on preparation methodology.

Both preleached mica edge orientations (Table 2) and rough basal surfaces (Fig. 14) showed appreciable reduction of U^{VI}. Consequently, we believe that uranyl can be heterogeneously reduced by ferrous micas under natural conditions. However, it is beyond the scope of this paper to ascertain the effect of preparation, if any, on quantitative reduction rates.

4.5.3. Fe oxidation state

Sample heterogeneity and analytical errors combine for Fe^{II}/Fe^{III} uncertainties on the order of 20%. For the low and medium Fe micas, $2U^{IV}/Fe$ values < 0.02 are well within the uncertainty of Fe^{II}/Fe^{III} analyses (Table 3; Raeburn et al., 1997), which would obscure evidence for differential oxidation of Fe in biotite between the experiments. It is only at high U^{IV} coverage that occurs on annite in a subset of the experiments that one would expect to see significant oxidation of Fe^{II} relative to annites with lower U^{IV} coverage. However, XPS analyses indicate no systematic trend in Fe^{II}/Fe^{III} as a function U^{IV}. Unfortunately, another source of error was discovered after the fact: exposure to the X-ray beam reduced Fe^{III} to Fe^{II}. Previous work by Raeburn et al. (1997) had indicated that only low Fe micas were susceptible to this kind of beam damage, so we did not think that this would be a problem with the annite. We now believe that the very low concentration of fluorine in the annite, a factor that contributed to its high reactivity with uranyl, also contributed to its beam sensitivity. As Fe analyses commenced anywhere from 30–60 min after uranium analyses, the effect of beam damage was likely severe and variable. Further, it is possible that beam damage rates and direction were a function of initial Fe^{III}/Fe^{II} ratios. In any case, this is an intrinsic problem because U^{VI} also reduces under the beam, so uranium analyses were always done first. Consequently, we consider Fe^{III}/Fe^{II} analyses unreliable.

4.6. Alternative Reduction Pathways

It is well documented that homogeneous reduction of U^{VI} by Fe^{II} in solution is kinetically hindered (e.g., Liger et al., 1999) and does not occur at laboratory time scales. However, still at issue is whether U^{VI} was sorbed and reduced by structural Fe^{II} or resorbed Fe^{II}. Large single crystals were used, which should have lowered the concentration of aqueous Fe derived from mica dissolution relative to powder experiments. Whereas, Fe must have dissolved, and XPS indicates this (Table 2), no aqueous Fe was detected by ICP. This should have appreciably lessened the interaction between U^{VI} and sorbed Fe^{II}, compared to powder experiments. To test this hypothesis the annite and lower Fe/Mg micas were put into the same solutions. If the dominant reaction was reduction of U^{VI} by non-structural Fe^{II} at edges, edge orientations of the different micas should have similar sorbed U^{IV}. This is a reasonable hypothesis given that

the structures for edge terminations are similar for all three micas. Consequently, that XPS analyses of edge orientations record orders-of-magnitude more U^{IV} sorbed to the annite relative to lower Fe/Mg micas, is consistent with structural Fe^{II} controlling U^{VI} reduction at edge sites. Further, if non-structural Fe^{II} was the active reducing agent, whether at edge or fixed charge sites, then for any given mica it would be reasonable to expect XPS to record a positive correlation between U^{IV} and Fe, due to intermingling or co-precipitation of sparingly soluble U^{IV} and Fe^{III} containing phases. In contrast, XPS analyses of edge orientations record that signal intensity for Fe, along with all mica components, diminishes with increasing U^{IV}. This too is consistent with structural Fe^{II}, not resorbed Fe^{II}, as the reducing agent.

That for any given mica U^{IV}/U^{VI} is much lower on exposed, smooth basal plane surfaces relative to edge orientations also is consistent with mineral compositional and crystallographic control of U^{VI} reduction rather than reduction of U^{VI} by resorbed Fe^{II}. However, the structural difference between the edge and exposed basal surfaces makes this argument less compelling than one based on comparison of edge orientations among the different micas.

5. CONCLUSIONS

Ferrous micas reduce U^{VI} heterogeneously under experimental conditions. Preleached micas and edge terminations on basal surfaces showed similar reactivity to unleached cut edge surfaces. This provides strong evidence that sorption/reduction of uranyl by micas should occur readily in nature, provided appropriate crystal chemical and solution compositions are present. The reaction is dependent on mica composition, pH, and the type and concentration of aqueous alkali cations. High Fe, low-F annite was particularly reactive, with reduction documented at U^{VI} concentrations as low as 0.5 μM and pH values from 4.5 to 9.5. Micas with lower Fe and higher F than the annite, showed demonstrable reactivity only when U^{VI} concentration reached 0.5 mM.

XPS analyses indicate that U^{VI} reduction occurs on edge but not on exposed basal surfaces, Na^+ promotes reduction, and K^+ suppresses reduction. XAS indicates that U^{VI} is partially reduced in the interlayer region. Total sorption and reduction peak around pH 6, in accord with batch sorption studies. In contrast, the reduction efficiency ($U^{IV}{}_{sorbed}/U^{VI}{}_{sorbed}$) is not a significant function of pH. This could imply competing processes that cancel, or that a pH effect is obscured by experimental/analytical errors. TEM records nano-scale U-rich zones in the interlayer region for those experiments with relatively high uranium sorption. The oxidation state of U in these zones is not known, but they are not associated with steps. Taken together, observations using different methodologies are consistent with reduction of U^{VI} in the interlayer region and at layer terminations by structural Fe^{II}.

Both XPS and XAS studies indicate that coupled sorption-reduction of U^{VI} depend on access of circulating fluids to mica edges. Regardless of P_{O_2} and P_{CO_2}, the reaction may not be an important process in systems with groundwaters that contain appreciable K or micas that contain high fluorine and Fe/(Fe + Mg) less than about 0.5. Importantly, reduction of sorbed U^{VI} was documented at pH 4.5 for the high-Fe low-F mica. Because reduction of U^{VI} by Fe^{II} adsorbed to mineral surfaces appears to require circum-neutral to basic pH (Liger et al., 1999), structural Fe^{II} in silicates could be particularly important in providing reduction pathways for U^{VI} in aqueous solutions at pH values appreciably less than neutral.

Acknowledgments—This research was supported by the Geosciences Research Program, Office of Basic Energy Sciences, U.S. Department of Energy. The PNC-CAT project is supported by funding from the U.S. Department of Energy, Basic Energy Sciences, and the Natural Sciences and Engineering Research Council in Canada. Use of the Advanced Photon Source was supported by the U.S. Department of Energy, Office of Science, Office of Basic Energy Sciences, under Contract No. W-31-109-ENG-38. Support by the DOE for this work does not constitute an endorsement by the DOE of the views expressed in this article. XPS was performed with the Scienta ESCA-300 X-ray photoelectron spectrometer housed in the Zettlemoyer Center for Surface Studies, Lehigh University. The authors thank Dr. Alfred Miller for guidance in the use of the XPS facility. We also thank three anonymous reviewers for their constructive comments.

Associate editor: E. H. Oelkers

REFERENCES

Ackay H. (1998) Aqueous speciation and pH effect on the sorption behavior of uranium by montmorillonite. *Radioanal. Nucl. Chem.* **237,** 133–137.

Acker J. G. and Bricker O. P. (1992) The influence of pH on biotite dissolution and alteration kinetics at low temperature. *Geochim. Cosmochim. Acta* **56,** 3073–3092.

Allard B., Rydberg J., Kipatsi H., and Torstenfelt B. (1979) Disposal of radioactive waste in granitic bedrock. In *Radioactive Waste in Geologic Storage* (ed. S. Fried). *Am. Chem. Soc. Symposium Series* **100,** 47–73.

Allen G. C. and Holmes N. R. (1987) Surface characterization of α, β, γ and δ-UO3 using X-ray photoelectron spectroscopy. *J. Chem. Soc. Dalton Trans.* 3009–3015.

Allen G. C. and Holmes N. R. (1993) Mixed valency behaviour in some uranium oxides studies by X-ray photoelectron spectroscopy. *Canadian J. of Appl. Spectr.* **38,** 124–130.

Allen G. C., Crofts J. A., Curtis M. T., Tucker P. M., Chadwick D. and Hampson P. J. (1974) X-ray photoelectron spectroscopy of some uranium oxide phases. *J. Chem. Soc. Dalton Trans.* 1296–1301.

Allen G. C., Tempest P. A., and Tyler W. T. (1987) Oxidation of crystalline UO_2 studied using X-ray photoelectron spectroscopy and X-ray diffraction. *J. Chem Soc. Faraday Trans.* **1,** 925–935.

Ames L. L., McGarrah J. E., Walker B. A., and Salter P. F. (1982) Sorption of uranium and cesium by Hanford basalts and associated secondary smectitite. *Chem. Geol.* **35,** 205–225.

Ames L. L., McGarrah J. E., and Walker B. A. (1983a) Sorption of trace constituents from aqueous solutions onto secondary minerals I. Uranium. *Clays Clay Minerals* **31,** 321–334.

Ames L. L., McGarrah J. E., and Walker B. A. (1983b) Sorption of uranium and radium by biotite, muscovite, and phlogopite. *Clays Clay Minerals* **31,** 343–351.

Amonette J. E. and Scott A. D. (1995) Oxidative weathering of trioctahedral micas by buffered H_2O_2 solutions. In *Clays Controlling the Environment (eds. G. J. Churchman, et al.), pp. 355–361. CSIRO Publishing, Melbourne, Australia.*

Andersson K., Torstenfelt B. and Allard B. (1982) Sorption behaviour of long-lived radionuclides in igneous rock. In *Proc. Symp. Env. Migration of Long-Lived Isotopes.* Vienna, IAEA.

Arnold T., Zorn T., Bernhard G., and Nitsche H. (1998) Sorption of uranium(VI) onto phyllite. *Chem. Geol.* **151,** 129–141.

Bargar J. R., Reitmeyer R., Lenhart J. J., and Davis J. A. (2000) Characterization of U(VI)-carbonato ternary complexes on hematite: EXAFS and electrophoretic mobility measurements. *Geochim. et Cosmochim. Acta* **64,** 2737–2749.

Berry J. A., Jeffries N. L. and Littleboy A. K. (1989) Studies of the near-surface spatial and depth distributions of uranium sorbed onto

granitic mineral assemblages. In *Proc. 6th Int. Symp. on Water-Rock Interaction*, Malvern, p. 75.

Berry J. A., Cowper M. M., Green A., Jeffries N. L. and Linklater C. M. (1991) Sorption of Radionuclides on Mineral Surfaces. *Proc. 3rd Int. Conf. on Nucl. Fuel Reprocessing and Waste Management*, Japan, p. 988.

Berry J. A., Bishop H. E., Cowper M. M., Fozard P. R., McMillan J. W., and Mountfort S. A. (1993) Measurement of the sorption of actinides on minerals using microanalytical techniques. *Analyst* **118,** 1241–1246.

Berry J. A., Bishop H. E., Cowper M. M., Fozard P. R., McMillan J. W., and Mountfort S. A. (1994) The use of microanalytic techniques to measure the distribution of uranium and plutonium sorbed on rocks and minerals. *Radiochim. Acta* **66/67,** 243–250.

Berry J. A., Bishop H. E., Cowper M. M., Fozard P. R., and McMillan J. W. (1995) The use of surface analytical techniques to measure the loadings of uranium and plutonium sorbed simultaneously from solution onto rocks. *Mater. Res. Soc. Symp. Proc.* **353,** 951–956.

Borovec Z. (1981) The adsorption of uranyl species by fine clay. *Chem. Geol.* **32,** 45–58.

Charlet L., Schindler L., Spadini L., Furrer G., and Zysset M. (1993) Cation adsorption on oxides and clays: The aluminum case. *Aquatic Sci.* **55,** 1015–1621.

Chisholm-Brause C., Conradson S. D., Eller P. G., and Morris D. E. (1992) Changes in U^{VI} speciation upon sorption onto montmorillonite from aqueous and organic solutions. *Mater. Res. Soc. Symp. Proc.* **257,** 315–322.

Chisholm-Brause C., Conradson S. D., Buscher C. T., Eller P. G., and Morris D. E. (1994) Speciation of uranyl sorbed at multiple binding sites on montmorillonite. *Geochim. Cosmochim. Acta* **58,** 3625–3631.

Dent A. J., Ramsay J. D. F., and Swanton S. W. (1992) An EXAFS study of uranyl ion in solution and sorbed onto silica and montmorillonite clay colloids. *J. Coll. Interf. Sci.* **150,** 45–60.

Dran J.-C., Mea D. G., Paccagnella A., Petit J.-C., and Menager M.-T. (1988) Sorption of actinide analogues on granite minerals studied by MeV ion beam techniques. *Radiochim. Acta* **44/45,** 299–304.

Eberly P. O., Janeczek J., and Ewing R. C. (1995) Precipitation of uraninite in chlorite-bearing veins of the hydrothermal alteration zone of the natural nuclear reactor at Bangombe, Republic of Gabon. *Materials Research Society Symposium Proceedings.* **353,** 1195–1202.

Eberly P. O., Ewing R. C., Janeczek J., and Furlano A. (1996) Clays at the natural reactor at Bangombe, Gabon: Migration of actinides. *Radiochim. Acta* **74,** 271–275.

Fanning D. S. and Keramidas V. Z. (1977) Micas. In *Minerals in Soil Environments* (eds. J. B. Dixon and S. B. Weed), pp. 221–257. Soil Science. Society of America.

Fiedor J. N., Bostic W. D., Jarabek R. J., and Farrell J. (1998) Understanding the mechanism of uranium removal from groundwater by zero-valent iron using X-ray photoelectron spectroscopy. *Environ. Sci. Technol.* **32,** 1466–1473.

Giaquinta D. M., Soderholm L., Yuchs S. E., and Wasserman S. R. (1997) The speciation of uranium in a smectite clay: Evidence for catalysed uranyl reduction. *Radiochim. Acta* **76,** 113–121.

Giblin A. M. (1980) The role of clay adsorption in genesis of uranium ores. In *Uranium in the Pine Creek Geosyncline* (eds. J. Ferguson and A. B. Goleby), pp. 521–529. IAEA.

Giblin A. M., Batts B. D., and Swaine D. J. (1981) Laboratory simulation of uranium mobility in natural waters. *Geochim. Cosmochim. Acta* **45,** 699–709.

Grenthe I. (1992) *Chemical Thermodynamics of Uranium*. North Holland, New York 715 pp.

Guilbert S., Guittet M. J., Barre N., Gautiier-Soyer M., Trocellier P., Gosset D., and Andriambololona Z. (2000) Dissolution of UO_2 in Boom clay water in oxidizing conditions: An XPS study. *J. of Nucl. Mater.* **282,** 75–82.

Guilbert S., Guittet M. J., Barre N., Trocellier P., Gautiier-Soyer M., Gosset D., and Andriambololona Z. (2002) Dissolution of uranium oxide in simulated Boom clay water. *Radiochim. Acta* **90,** 75–80.

Heald S., Stern E. A., Brewe D., Gordon R. A., Crozier E. D., Jiang D., and Cross J. O. (2001) XAFS at the Pacific Northwest Consortium-Collaborative Access Team Undulator Beamline. *J. Synchrotron Rad.* **8,** 342–344.

Hedhili M. N., Yakshinskiy B. V., and Madey T. E. (2000) Interaction of water vapor with UO_2(001). *Surface Science* **445,** 512–525.

Hennig C., Reich T., and Scheidegger A. M. (2002) Structure of uranium sorption complexes at montmorillonite edge sites. *Radiochim. Acta* **90,** 653–657.

Hochella M. F. and Jr. (1988) Auger electron and X-ray photoelectron spectroscopies. In *Spectroscopic Methods in Mineralogy and Geology* (ed. F. C. Hawthorne), pp. 573–630. Mineralogical Society of America, Washington, D.C.

Hudson E. A., Terminello L. J., Viani B. E., and Reich T. (1994) X-ray absorption studies of uranium sorption on mineral substrates. In Application of Synchotron Radiation Techniques to Materials Science (Terminello L. J., Shinn N. D., Ice G. E., D'Amico K. L. and Perry D. L., Eds.), *Mater. Res. Soc. Symp. Proc.* **375,** 235–240.

Hudson E. A., Terminello L. J., Viani B. E., and Reich T. (1999) The structure of U^{6+} sorption complexes on vermiculite and hydrobiotite. *Clays Clay Minerals* **375,** 439–457.

Idemitsu K., Obata K., Furuya H., and Inagaki Y. (1995) Sorption behavior of uranium^{VI} on a biotite mineral. *Mater. Res. Soc. Symp. Proc.* **353,** 981–988.

Ilton E. S. and Veblen D. R. (1994) Chromium sorption by phlogopite and biotite in acidic solutions at 25° C: Insights from X-ray photoelectron spectroscopy and electron microscopy. *Geochim. Cosmochim. Acta* **58,** 2777–2788.

Ilton E. S., Veblen D. R., Moses C. O., and Raeburn S. P. (1997) The catalytic effect of sodium and lithium ions on coupled sorption-reduction of chromate at the biotite edge-fluid interface. *Geochim. Cosmochim. Acta* **61,** 3543–3563.

Ilton E. S., Moses C. O., and Veblen D. R. (2000) Using X-ray photoelectron spectroscopy to discriminate among different sorption sites of micas. With implications for heterogeneous reduction of chromate at the mica-water interface. *Geochim. Cosmochim. Acta* **64,** 1437–1450.

Langmuir D. (1978) Uranium solution-mineral equilibria at low temperatures with applications to sedimentary ore deposits. *Geochim. Cosmochim. Acta* **42,** 571–580.

Liger E., Charlet L., and Capellen P. V. (1999) Surface catalysis of uranium(VI) reduction by iron(II). *Geochim. Cosmochim. Acta* **63,** 2939–2955.

Mainka G., Zorn T., Arnold T., and Bernhard G. (1999) Distribution of uranium(VI) on biotite surfaces. *Wiss. Ber.-forschungszent. Karlsruhe* **6291,** 83–85.

McKinley I. G. and Scholtis A. (1993) A comparison of radionuclide sorption databases used in recent performance assessments. *J. Contam. Hydrol.* **13,** 347–363.

McKinley J. P., Zachara J. M., Smith S. C., and Turner G. D. (1995) The influence of uranyl hydrolysis and multiple site–binding reactions of adsorption of U^{VI} to montmorillonite. *Clays Clay Minerals* **43,** 586–598.

Morris D. E., Chisholm-Brause C., Barr M. E., Conradson S. D., and Eller P. G. (1994) Optical spectroscopic studies of the sorption of UO_2^{2+} species on a reference smectite. *Geochim. Cosmochim. Acta* **58,** 3613–3623.

Morris D. E., McKinley J. P., Smith S. C. and Zachara J. M. (1997) Uranyl surface complexation on smectites: Combining optical spectroscopic studies with modeling. *213th Am. Chem. Soc. Nat. Meeting Abstracts with Progams*.

Moyes L. N., Parkman R. H., Charnock J. M., Vaughan D. J., Livens F. R., Hughes C. R., and Braithwaite A. (2000) Uranium uptake from aqueous solution by interaction with goethite, lepidocrocite, muscovite, and mackinawite: An X-ray absorption spectroscopy study. *Environ. Sci. Technol.* **34,** 1062–1068.

Nero M. D., Salah S., Miura T., Clement A., and Gauthier-Lafaye F. (1999) Sorption desorption processes of uranium in clayey samples of the Bangombe natural reactor zone, Gabon. *Radiochim. Acta* **87,** 135.

O'Loughlin E. J., Kelly S. D., Cook R. E., Csencsits R., and Kemner K. M. (2003) Reduction of uanium(VI) by mixed iron(II)/iron(II) hydroxide (green rust): Formation of UO_2 nanoparticles. *Environ. Sci. Technol.* **37,** 721–727.

Pabalan R. T. and Turner D. R. (1997) Uranium(VI) sorption on montmorillonite: Experimental and surface complexation modeling study. *Aquat. Geochem.* **2,** 203–226.

Pabalan R. T., Turner D. R., Bertetti F. P., and Prikryl J. D. (1998) Uranium(VI) sorption onto selected mineral surfaces. In *Adsorption of Metals by Geomedia* (ed. E. A. Jenne), pp. 99–130. Academic, San Diego, CA.

Pireaux J. J., Riga J., Thibaut E., Tenret-Noel C., Caudano R., and Verbist J. J. (1977) Shake-up satellites in the x-ray photoelectron spectra of uranium oxides and fluorides. A band structure scheme for uranium dioxide, UO_2. *Chem. Phys.* **22,** 113–120.

Prikryl J. D., Jain A., Turner D. R., and Pabalan R. T. (2001) Uranium^{VI} sorption behavior on silicate mineral mixtures. *J. Contaminant Hydrol.* **47,** 241–253.

Raeburn S. P., Ilton E. S., and Veblen D. R. (1997) Quantitative determination of the oxidation state of iron in biotite by X-ray photoelectron microscopy. I. Calibration. *Geochim. Cosmochim. Acta* **61,** 4519–4530.

Redden G. D., Persson P. and Bencheikh-Latmani R. (1997) Adsorption of uranyl on gibbsite, kaolinite and goethite in the presence of citric acid. Proton stoichiometry and IR spectroscopic details for the goethite system. *213th Am. Chem. Soc. Nat. Meeting, Abstracts with Progams*.

Scofield J. H. (1976) Hartree-Slater subshell photoionization cross-sections at 1254 and 1457 eV. *J. Electron Spectrosc.* **8,** 129–137.

Scott A. D. and Amonette J. (1988) The role of iron in mica weathering. *NATO ASI Ser. C.* **217,** 537–623.

Seah M. P. and Dench W. A. (1979) Quantitative electron spectroscopy of surfaces: A standard data base for electron inelastic mean free paths in solids. *Surface Interface Anal.* **1,** 2–11.

Shirley D. A. (1972) High resolution X-ray photoemission spectrum of the valence bands of gold. *Phys. Rev.* **B5,** 4709–4714.

Smyth J. R., Thompson J., and Wolfsberg K. (1980) Microautographic studies of the sorption of U and Am on natural rock samples. *Radioactive Waste Manag.* **1,** 13–24.

Sposito G. (1984) *The Surface Chemistry of Soils*. Oxford University Press, New York.

Sunder S, Miller N. H (1995) XPS, XRD and SEM study of oxidation of UO_2 by air in gamma radiation at 150° C. *AECL-11351.* COG. 95–296.

Sunder S., Shoesmith D. W., Bailey M. G., Stanchell F. W., and McIntyre N. S. (1981) Anodic oxidation of UO_2. Part 1. Electrochemical and X-ray photoelectron spectroscopic studies in neutral solutions. *J. Electroanal. Chem.* **130,** 163–179.

Sunder S., Boyer G. D., and Miller N. H. (1990) XPS studies of UO_2 oxidation by alpha-radiolysis of water at 100° C. *J. Nucl. Mater.* **175,** 163–169.

Sunder S., Cramer J. J., and Miller N. H. (1992) X-ray photoelectron spectroscopic study of uranium minerals from the Cigar Lake uranium deposit. In *Scientific Basis for Nuclear Waste Management* (ed. C. G. Sombret). *Mater. Res. Soc. Symp. Proc.* **257,** 449–457.

Sunder S., Miller N. H., and Duclos A. M. (1994) XPS and XRD studies of samples from the natural fission reactors in the Oklo uranium deposits. *Mater. Res. Soc. Symp. Proc.* **333,** 631–638.

Sunder S., Cramer J. J., and Miller N. H. (1996) Geochemistry of the Cigar Lake uranium deposit: XPS studies. *Radiochim. Acta* **74,** 303–307.

Syed H. S. (1999) Comparison studies of adsorption of thorium and uranium on pure clay minerals and local Malaysian soil sediments. *J. Radioanal. Nucl. Chem.* **241,** 11.

Sylwester E. R., Hudson E. A., and Allen P. G. (2000) The structure of uranium (U(VI)) sorption complexes on silica, alumina, and montmorillonite. *Geochim. Cosmochim. Acta* **64,** 2431–2438.

Thompson H. A., Parks G. A., and Brown G. E., Jr. (1998) Structure and composition of uranium^{VI} sorption complexes at the kaolinite-water interface. In *Adsorption of Metals by Geomedia* (ed. E. A. Jenne), pp. 349–370. Academic Press, San Diego.

Ticknor K. V. (1994) Uranium sorption on geological materials. *Radiochim. Acta* **64,** 229–236.

Ticknor K. V., Vilks P., and Vandergraaf T. T. (1996) The effect of fulvic acid on the sorption of actinides and fission products on granite and selected minerals. *Appl. Geochem.* **11,** 555–556.

Tsunashima A., Brindley G. W., and Bastovanov M. (1981) Adsorption of uranium from solutions by montmorillonite; compositions and properties of uranyl montmorillonites. *Clays Clay Minerals* **29,** 10–16.

Turner G. D., Zachara J. M., McKinley J. P., and Smith S. C. (1996) Surface-charge properties and UO_2^{2+} adsorption of a subsurface smectite. *Geochim. Cosmochim. Acta* **60,** 3399–3414.

Van den Berghe S., Miserque F., Gouder T., Gaudreau B., and Verwerft M. (2001) X-ray photoelectron spectroscopy on uranium oxides: A comparison between bulk and thin layers. *J. of Nuclear Materials* **294,** 168–174.

Vandergraaf T. T., Ticknor K. V., and Melnyk T. W. (1993) The selection of a sorption data base for the geosphere model in the Canadian Nuclear Fuel Waste Management Program. *J. Contam. Hydrol.* **13,** 327–345.

Wersin P., Hochella M. F., Jr, Person P., Redden G., Leckie J. O., and Harris D. W. (1994) Interaction between aqueous uranium^{VI} and sulfide minerals: Spectroscopic evidence for sorption and reduction. *Geochim. Cosmochim. Acta* **58,** 2829–2843.

White A. F. (1990) Heterogeneous electrochemical reactions associated with oxidation of ferrous oxide and silicate surfaces. In *Mineral-Water Interface Geochemistry* (eds. M. F. Hochella, Jr. and A. F. White), pp. 467–510, Mineralogical. Society of America, Washington, D.C.

White A. F. and Yee A. (1985) Aqueous oxidation-reduction kinetics associated with coupled electron-cation transfer from iron-containing silicates at 25°C. *Geochim. Cosmochim. Acta* **49,** 1263–1275.

APPENDIX

Apparent U overlayer thickness was calculated by $D = -\lambda\ln(1-I_x/I)$, where D is the overlayer thickness, λ is the escape depth for U4f photoelectrons in uraninite (see Hochella, 1988 for definition), I_x is the signal from the overlayer, and I is the signal from an infinity thick uraninite. This equation is a special case of a more general equation given by others including Hochella (1988). λ was set at 15 A, which is in the lower range for U4f photoelectrons traversing inorganic compounds (Seah and Dench, 1979). Assumptions include a continuous and uniform overlayer, and no contribution from U in the mica substrate. The equation is not applicable when the overlayer thickness approaches the bulk material; consequently, calculations were limited to moderate to low values of U/Si. Additional uncertainties were introduced by the use of a partially hydrated, mildly oxidized uraninite for the infinitely thick material, and differences in C overlayer thickness between the uraninite and experimental samples.